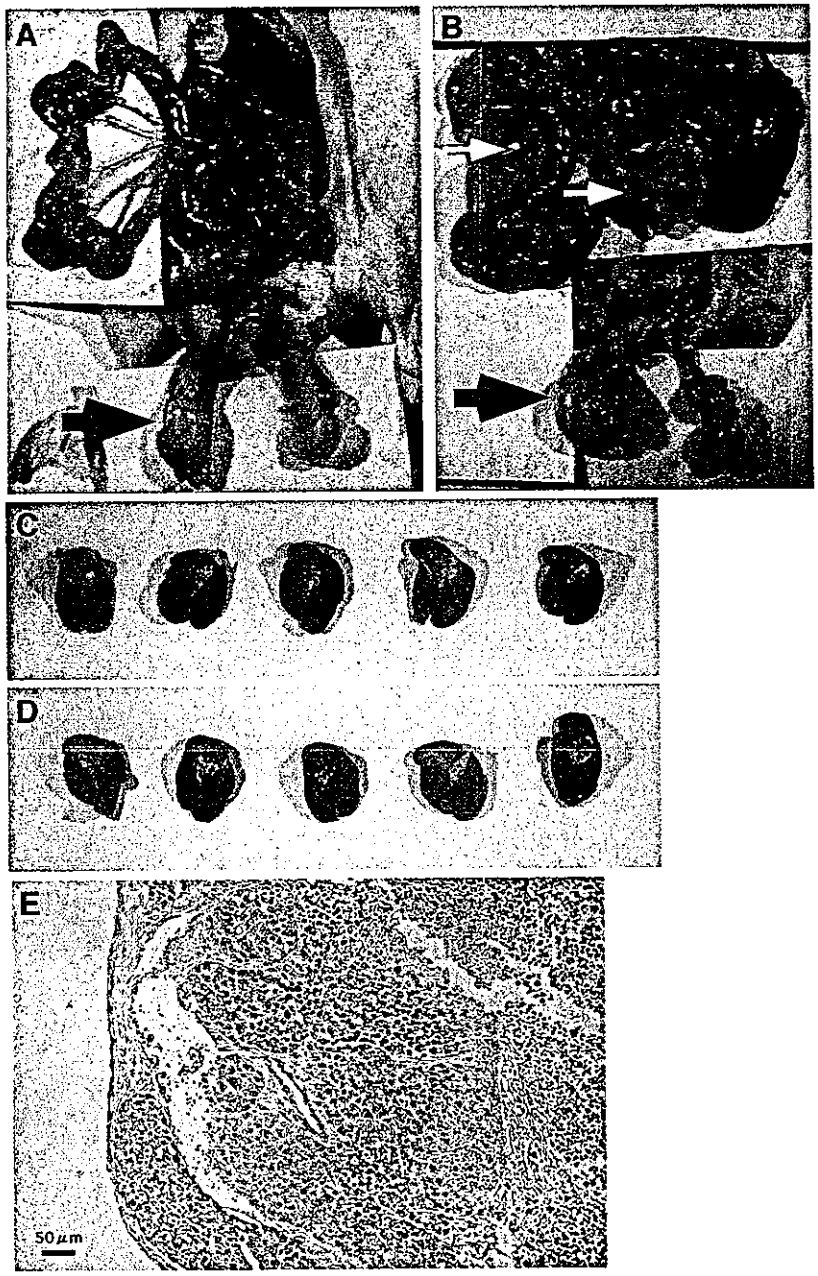

Fig. 5. Tumor formation by JKT-1-Tro cells in the nude mice. JKT-1-mock cells (*A*) and JKT-1-Tro-1 cells (*B*; 2×10^6cells each) were inoculated in the right testis. JKT-1-Tro-1 cells produced intra-abdominal metastasis in all of the mice ($n = 5$; *B*), whereas JKT-1-mock cells produced no metastasis ($n = 5$; *A*). No differences in the size of testes were seen between JKT-1-mock and JKT-1-Tro (*black arrows*). Note that JKT-1-Tro-1 produces numerous mesenteric metastases (*open arrows in B*). JKT-1 mock (*C*) or JKT-1-Tro-1 (*D*) produced no lung metastasis. JKT-1-Tro-2 cells showed also the same result as JKT-1-Tro-1 (data not shown). *E*, immunohistochemistry of metastasized tumor with antitrophinin antibody.

cell surface, whereas two clones for JKT-1-mock do not (Fig. 3*B*). Thus, clonal variations among JKT-1-Tro and those among JKT-1-mock are considered to be minimum.

Because malignancy is closely associated with cell proliferation activity, we determined cell numbers of JKT-1-Tro cells and JKT-1-mock cells. The results show no significant difference between JKT-1-Tro cells and JKT-1-mock cells in cell numbers during *in vitro* culture (data not shown), suggesting that acquisition of trophinin does not solely enhance cell proliferation activity of JKT-1 cells cultured *in vitro*.

Next, JKT-1-Tro cells and JKT-1-mock cells were subjected to motility and invasion assays using a transwell cell culture system. Fibronectin and Matrigel were coated on the lower and upper face of the transwell for testing motility and invasion, respectively. These assays revealed that JKT-1-Tro cells are significantly mobile (Fig. 4*A*) and invasive (Fig. 4*B*) compared with JKT-1-mock cells. The possibility for clonal deviations of these results is excluded, because the differences between JKT-1-Tro clones were not significant.

Metastatic Potential of JKT-1-Tro Cells *in Vivo* in the Mouse. Because clinical data (Table 1) indicated a strong correlation between trophinin-positive testicular tumors and lung metastasis, we tested whether JKT-1-Tro cells metastasize to the lung in the mouse. JKT-1-Tro cells and JKT-1-mock cells were inoculated in the right testis of the nude mice. Three weeks after inoculation, mice were sacrificed to determine the tumor size and metastasis. JKT-1-Tro cells produced massive intra-abdominal metastasis in all of the mice ($n = 5$), whereas mock transfectants produced no metastasis ($n = 5$; Fig. 5, *A* and *B*). Although the lung metastasis is common in the cancer patients, evidence for the lung metastasis has not been obtained by these experiments (Fig. 5, *C* and *D*). Immunohistochemistry using monoclonal antitrophinin antibody showed that mesenteric metastases produced in the mouse were positive for trophinin (Fig. 5*E*).

Although the experiments using the mice did not show the lung metastasis, the lung metastasis and trophinin expression are hallmark in the testicular cancers in humans (Table 1). To gain insight into the mechanisms for lung metastasis of trophinin-positive testicular germ

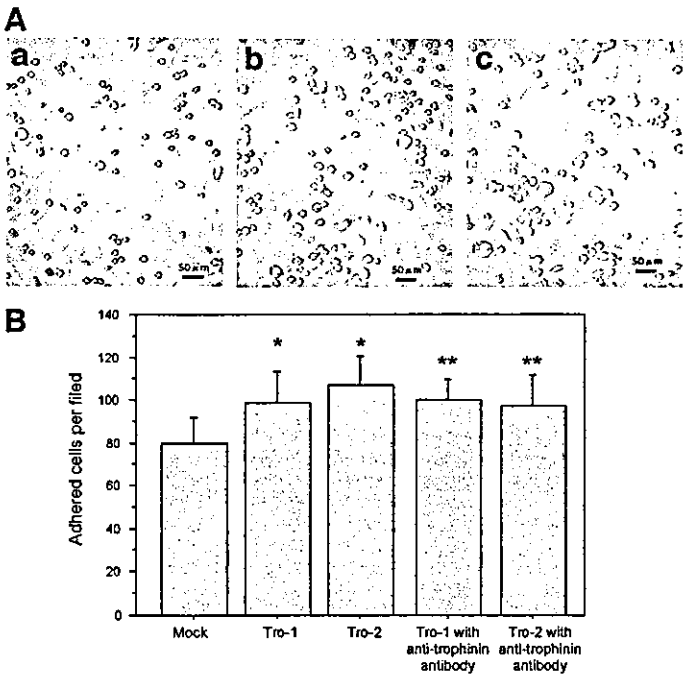

Fig. 6. Adhesion of mock transfectants and JKT-1-Tro cells to human lung microvascular endothelial cells (HMVEC-L). *A*, representative photomicrographs of JKT-1-Tro cells adhered to HMVEC-L. Each shows (*panel a*) mock transfectants adhered to HMVEC-L, (*panel b*) JKT-1-Tro-1 cells adhered to HMVEC-L, and (*panel c*) JKT-1-Tro-1 cells pretreated with antitrophinin antibody and adhered to HMVEC-L. JKT-1-Tro-2 cells showed the same result as JKT-1-Tro-1 (data not shown). *B*, numbers of JKT-1-Tro cells adhered to the HMVEC-L. *, statistical significance between JKT-1-Tro and the mock-transfectant cells ($P < 0.001$, Mann-Whitney *U* test). Note that there are no effects of antitrophinin antibody on the adhesion of JKT-1-Tro-1 and -2 cells. * *, statistical significance with or without antitrophinin antibody treatment. ($P = 0.3$, Mann-Whitney *U* test); *bars*, ±SD.

cell tumors, we compared the adhesion of JKT-1-Tro cells and JKT-1-mock cells to human lung microvascular endothelial cells by cell adhesion assay *in vitro*. As shown in Fig. 6, JKT-1-Tro cells were only slightly more adhesive to HMVEC-L than JKT-1-mock cells, whereas antitrophinin antibody had no effect on the adhesion between JKT-1-Tro cells and HMVEC-L (Fig. 6). These results suggest that trophinin is not the factor determining the adhesion of tumor cells to HMVEC-L.

DISCUSSION

Testicular germ cell tumor is one of the few neoplasms associated with accurate serum marker, hCG (6). The hCG is found in the placenta in pregnant women (18) but not in any tissue from healthy men. This allows careful follow-up in men with testicular germ cell tumor early in the course of the disease (19, 20). In germ cell tumors and the placenta, syncytiotrophoblastic cells are responsible for the production of hCG. Although both human and mouse produce testicular germ cell tumors, spontaneous trophoblastic transformation of cancer cells does not naturally occur in the mouse (21). Thus, in humans, trophoblastic transformation occurs in the breast, prostate, bladder, thyroid, colon, lung, and endometrial cancers (22–24).

Studies on embryo implantation have revealed significant differences of this process among mammals (25). Remarkably, ectopic pregnancy occurring at a rate as high as 1.4% in all of the pregnancies in humans (26, 27) does not occur naturally or experimentally in other animals, including nonhuman primates (28–30). As described below, trophoblastic transformation of tumors in humans may be explained by the uniqueness of the β subunit of hCG (11, 31).

The hCG is a 38-kDa glycoprotein hormone composed of α and β polypeptide chains (7). The hCG and its pituitary counterpart, lutropin, comprise a family of heterodimeric glycoprotein hormones, including follitropin and thyrotropin, that share a common α subunit but differ in their hormone-specific β subunit (7). The gene encoding CG-α is homologous to those encoding thyroid-stimulating hormones, of which the structures are evolutionally conserved among wide variety of animals (32). By contrast, CG-β subunit is specific to primates, and human CG-β gene is diverged from the CG-β genes of nonhuman primates (31).

Trophinin mediates homophilic cell adhesion between human trophoblastic cells and endometrial epithelial cells at their respective apical cell surfaces (8, 9). Strong expression of trophinin was found at the human embryo implantation site (14). Trophinin is also expressed during ectopic pregnancies (11). Interestingly, trophinin expression by the fallopian tubal epithelia depends on the existence of implanting embryo. Thus, the maternal epithelia adjacent to the implantation site express trophinin strongly, whereas the maternal cells a few millimeters away from the implantation site barely express trophinin (11). Such spatially restricted trophinin expression suggests the existence of an embryo-derived factor that stimulates the maternal cells for trophinin expression. This embryonic factor may be CG-β, which is secreted from the trophectoderm of the blastocyst (33–35), because the fallopian tubal explants incubated with hCG showed the elevation of trophinin transcripts (11).

In this study, we found that testicular germ cell tumors often express trophinin (Table 1; Figs. 1 and 2). It is noteworthy that trophinin expression positively correlates with the malignancy of testicular tumor, particularly with the metastasis (Table 1). Our data also showed positive correlation between trophinin expression and hCG-β in the sera of the patients (Table 1; Fig. 1). Taken together, hCG-β expressed by human cancer cells might act on the cancer cells in an autocrine manner to induce trophinin expression.

In this study, we showed that ectopic expression of trophinin in JKT-1 cells enhances motility and invasiveness of the cells *in vitro* (Fig. 4). When JKT-1-Tro cells were inoculated into the mouse, they showed massive peritoneal metastasis (Fig. 5). Clinical data of the testicular germ cell tumors (Table 1) showed that testicular germ cell tumors metastasize to the lung (36). This suggested a possibility that trophinin enhances the lung metastasis. However, our experiments using JKT-1-Tro cells did not show the lung metastasis in the mouse (Fig. 5). Such an apparent discrepancy between the mouse experiments and clinical observations may be explained by the expression of tastin and bystin in the lung metastasized tumors (data not shown). The mechanism underlying the lung metastasis of these tumors remains to be defined in the future study.

Because we identified trophinin, tastin, and bystin as proteins with potential involvement in embryo implantation (8–10), functions of these proteins other than cell adhesion has not been described. Because trophinin, tastin, and bystin are expressed in the human placenta during the periods of early stage of placental development (14), it is possible that these proteins are involved in the subsequent trophoblast invasion process triggered by the initial cell adhesion. Therefore, present study is the first to provide with a suggestion that trophinin plays a role in invasion. Future studies should define the mechanisms of how trophinin promotes cellular motility in embryo implantation and cancer metastasis. The information obtained by such studies will help in designing a therapy against trophoblastic neoplasm, including testicular germ cell tumor.

ACKNOWLEDGMENTS

We thank Dr. Elise Lamar for editing the manuscript and Aleli Morse for her secretarial assistance.

REFERENCES

1. Richie JP. Neoplasms of the testis. In: Walsh PC, Retik AB, Vaughan ED, Wein AJ, editors. Campbell's urology. Vol 3. Philadelphia: WB Saunders; p. 2411–52.
2. Huyghe E, Matsuda T, Thonneau P. Increasing incidence of testicular cancer worldwide: a review. J Urol 2003;170:5–11.
3. Merguerian PA. Pediatric genitourinary tumors. Curr Opin Oncol 2003;15:222–6.
4. Gholam D, Fizazi K, Terrier-Lacombe MJ, et al. Advanced seminoma–treatment results and prognostic factors for survival after first-line, cisplatin-based chemotherapy and for patients with recurrent disease: a single-institution experience in 145 patients. Cancer (Phila) 2003;98:745–52.
5. Christian JA, Huddart RA, Norman A, et al. Intensive induction chemotherapy with CBOP/BEP in patients with poor prognosis germ cell tumors. J Clin Oncol 2003;21: 871–7.
6. Madersbacher S, Gerth R, Mann K, Dirnhofer S, Berger P. Gonadotrophin secretion patterns in testicular cancer patients with greatly increased human chorionic gonadotrophin serum concentrations. J Endocrinol 1998;159:451–8.
7. Pierce J, Parsons TF. Glycoprotein hormones: structure and Function. Annu Rev Biochem 1981;50:465–95.
8. Fukuda MN, Sato T, Nakayama J, et al. Trophinin and tastin, a novel cell adhesion complex with potential involvement in embryo implantation. Genes Dev 1995;9: 1199–210.
9. Suzuki N, Zara J, Sato T, et al. A novel cytoplasmic protein, bystin, interacts with trophinin, tastin, and cytokeratin, and may be involved in trophinin mediated cell adhesion between trophoblast and endometrial epithelial cells. Proc Natl Acad Sci USA 1998;95:5027–32.
10. Fukuda MN, Nozawa S. Trophinin, tastin, and bystin: a complex mediating unique attachment between trophoblastic and endometrial epithelial cells at their respective apical cell membranes. Semin Reprod Endocrinol 1999;17:229–34.
11. Nakayama J, Aoki D, Suga T, et al. Implantation-dependent expression of trophinin by maternal fallopian tube epithelia during tubal pregnancies: possible role of human chorionic gonadotrophin on ectopic pregnancy. Am J Pathol 2003;163:2211–9.
12. Denker H-W. Trophoblast-endometrial interactions at embryo implantation: a cell biological paradox. In: Denker H-W, Aplin JD, editors. Trophoblast research. New York: Plenum Medical Book Company; 1990. p. 3–20.
13. Greene FL, Page DL, Fleming ID, et al., editors. AJCC cancer staging manual. Edition 6. New York: Springer-Verlag; 2002. p. 317–22.
14. Suzuki N, Nakayama J, Shih I-M, et al. Expression of trophinin, tastin, and bystin by trophoblast and endometrial cells in human placenta. Biol Reprod 1999;60:621–7.
15. Kinugawa K, Hyodo F, Matsuki T, et al. Establishment and characterization of a new human testicular seminoma cell line, JKT-1. Int J Urol 1998;5:282–7.
16. Albini A, Iwamoto Y, Kleiman HK, et al. A rapid in vitro assay for quntitating the invasive potential of tumor cells. Cancer Res 1987;47:3239–45.
17. Sobin LH, Fleming ID. TNM classification of malignant tumors. Edition 5. Union Internationale Contre le Cancer and the American Joint Committee on Cancer. Cancer (Phila) 1997;80:1803–4.
18. Wilcox AJ, Baird DD, Weinberg CR. The time of implantation of the conceptus and loss of pregnancy. N Engl J Med 1999;340:1796–9.
19. Mazumdar M, Bajorin DF, Bacik J, et al. Predicting outcome to chemotherapy in patients with germ cell tumors: the value of the rate of decline of human chorionic gonadotrophin and alpha-fetoprotein during therapy. J Clin Oncol 2001;19:2534–41.
20. Bellet D, Bidart JM, Jolivet M. A monoclonal antibody against a synthetic peptide is specific for the free native human chorionic gonadotropin beta-subunit. Endocrinology 1984;115:330–6.
21. Tanaka S, Kunath T, Hadjantonakis AK, Nagy A, Rossant J. Promotion of trophoblast stem cell proliferation by FGF4. Science (Wash DC) 1998;282:2072–5.
22. Lehtovirta P, Alfthan H, Vaetiainen J, Stenman U. Skin metastases of gynecological adenocarcinomas affecr serum levels of hCG beta but not those of SCC antigen. Tumor Biol 1999;20:251–5.
23. Konishi I, Kuroda H, Mandai M. Gonadotropins and development of ovarian cancer. Oncology 1999;57:45–8.
24. Bellet D, Lazar V, Bieche I, et al. Malignant transformation of nontrophoblastic cells is associated with the expression of chorionic gonadotropin beta genes normally transcribed in trophoblastic cells. Cancer Res 1997;57:516–23.
25. Carson DD, Bagchi I, Dey SK, et al. Embryo implantation. Dev Biol 2000;223:217–37.
26. Brenner PF, Roy S, Mishell DR Jr. Ectopic pregnancy. A study of 300 consecutive surgically treated cases. J Am Med Assoc 1980;243:673–6.
27. Graczykowski JW, Mishell DRJ. Ectopic pregnancy. In: Lobo RA, Mishell DRJ, Paulson RJ, Shoupe D, editors. Mishell's textbook of infertility, contraception, and reproductive endocrinology. Massachusetts: Blackwell Science; 1997. p. 623–37.
28. Orsini MW, McLaren A. Loss of the zona pellucida in mice, and the effect of tubal ligation and ovariectomy. J Reprod Fertil 1967;13:485–99.
29. Tutton DA, Curr DH. The fate of trophoblast within the oviduct in the mouse. Gynecol Obstet Investig 1984;17:18–24.
30. Pauerstein CJ, Eddy CA, Koong MK, Moore GD. Rabbit endosalpinx suppress ectopic implantation. Fertil Steril 1990;54:522–6.
31. Talmadge K, Vamvakopouics WC, Fiddes JC. Evolution of the genes for the subunits of human chorionic gonadotropin and luteinizing hormone. Nature (Lond) 1984;307: 37–40.
32. Li MD, Ford JI. A comprehensive evolutionary analysis based on nucleotide and amino acid sequences of the a- and b-subunits of glycoprotein hormone gene family. J Endocrinol 1998;156:529–42.
33. Jurisicova A, Antenos M, Kapasi K, Meriano J, Casper RF. Ability in the expression of trophectodermal markers b-human chorionic gonadotrophin, human leukocyte antigen-G and pregnancy specific b-1 glycoprotein by the human blastocyst. Human Reprod 1999;14:1852–8.
34. Lopata A, Oliva K, Stanton PG, Robertson DM. Analysis of chorionic gonadotrophin secreted by cultured human blastocysts. Mol Hum Reprod 1997;3:517–21.
35. Licht P, Russu V, Wildt L. On the role of human chorionic gonadotropin (hCG) in the embryo-endometrial microenvironment: implications for differentiation and implantation. Semin Reprod Med 2001;19:37–47.
36. Suita S, Shono K, Tajiri T, et al. Malignant germ cell tumors: clinical characteristics, treatment, and outcome. A report from the study group for Pediatric Solid Malignant Tumors in the Kyushu Area, Japan. J Pediatr Surg 2002;37:1703–6.

Polysialic acid and HNK-1 are expressed in the adult rat vestibular endorgans

Manami Isawa, Yutaka Takumi, Shigenari Hashimoto, Jun Nakayama[1] and Shin-ichi Usami[CA]

Departments of Otorhinolaryngology; [1]Pathology, Shinshu University School of Medicine, 3-1-1 Asahi, Matsumoto 390-8621, Japan

[CA]Corresponding Author: usami@hsp.md.shinshu-u.ac.jp

Received 12 February 2004; accepted 31 March 2004

DOI: 10.1097/01.wnr.0000134585.87335.0d

Polysialic acid (PSA) and human natural killer (HNK)-1 carbohydrate epitopes are expressed mainly in developing neurons but also in restricted areas, even in adulthood. In the present study, we demonstrated the expression of PSA and HNK-1 epitopes in adult primary vestibular afferent neurons. In addition, we confirmed the presence of two distinct polysialyltransferases, PST and STX, that form PSA, as well as two types of glucuronyltransferases, GlcAT-P and GlcAT-S involved in the biosynthesis of HNK-1 epitopes in the vestibular endorgans. These results combined suggest that both PSA and HNK-1 carbohydrate epitopes are synthesized and may have an important role in the adult peripheral vestibular endorgans. *NeuroReport* 15:1575–1578 © 2004 Lippincott Williams & Wilkins.

Key words: Human natural killer (HNK)-1 carbohydrate epitope; Neural cell adhesion molecule (NCAM); Polysialic acid (PSA); Vestibular endorgans

INTRODUCTION

Neural cell adhesion molecule (NCAM) regulates cell to cell or cell to substrate interactions, and the polysialylated form of NCAM associated with an α-2,8-linked polysialic acid (PSA) reduces the adhesive capacity of NCAM, thus allowing neuronal migration [1–3] (Fig. 1). Consequently, the polysialylated form of NCAM (PSA-NCAM) is considered to play a crucial role in neural development as well as in neuronal plasticity. Another type of glycan, human natural killer (HNK)-1 carbohydrate epitope attached to NCAM is also considered to be involved in neuronal structural plasticity [4] (Fig. 1). Neuronal migration occurs during the embryonic stage, and neural rearrangement is completed by the early postnatal stage. However, in the adult, neural rearrangement/plasticity still remains only in restricted regions that continue to undergo structural rearrangement such as the hippocampus and olfactory bulb [5]. A recent study revealed that the cochlea is also one of the organs where PSA-NCAM continues to be expressed even in adulthood [6], and suggested the potential role of synaptic rearrangement. The vestibular endorgans (otolith organs and semicircular canals) and other sensory organs situated in the inner ear, detect linear and angular accelerations of the body and send this information to the brain via the primary afferent neurons (vestibular ganglion cells). It is an interesting question whether the vestibular endorgans are equipped with similar characteristic features, because they are evolutionarily analogous to, and may be structurally homologous with, the cochlea. In the current study, the presence and localization of PSA-NCAM and HNK-1 carbohydrate epitope in the adult rat were investigated. In addition, we examined the expression of two polysialyltransferases, PST (ST8Sia IV) and STX (ST8Sia II) [7], as well as two glucuronyltransferases, GlcAT-P and GlcAT-S [8,9] that form PSA and HNK-1 carbohydrate epitopes, respectively.

MATERIALS AND METHODS

Animals: Male Wistar rats aged 8 weeks, weighing 270–290 g were used. All animal handling procedures were in accordance with a protocol approved by the Ethics Committee of Shinshu University School of Medicine. All animal experimentation was approved by the Institutional Animal Care and Utilization Committee of Shinshu University School of Medicine.

Immunocytochemistry: Animals were anesthetized with sodium pentobarbital (Nembutal, 50 mg/kg). After intracardial perfusion with 4% paraformaldehyde in 0.1 M phosphate buffer saline (PBS) pH 7.4, the vestibular endorgans and the hippocampus were rapidly removed and fixed with the same fixative for 6–8 h at 4°C. The cryosections were immunostained with the following primary/secondary antibody combinations: (1) rat monoclonal anti-PSA (12F8; PharMingen; 1 μg/μl)/biotinylated anti-rat IgG (Amersham, 1:200) and streptavidin fluorescein (FITC; Amersham, 1:250); (2) mouse monoclonal anti-HNK-1 carbohydrate epitope (HNK-1; Becton Dickinson; 1 μg/μl)/goat anti-mouse TRITC (Leinco Technologies, 1:150); (3) rabbit polyclonal anti-neurofilament 200 (Sigma; 1 μg/μl)/goat anti-rabbit TRITC (Leinco Technologies, 1:150). The specimens were examined with a confocal scanning

microscope (Olympus BX50) equipped with the appropriate filter combinations.

Reverse transcription-polymerase chain reaction (RT-PCR) analysis: Total RNA was extracted from vestibular end organs including three semicircular canals, two maculae and the vestibular ganglion with the acid guanidium-phenol-chloroform method using 4 M guanidine thiocyanate (Wako), 25 mM sodium citrate (Wako), and 0.5% N-lauroylsarcosine (Wako). RT-PCR was performed with the aid of an RNA PCR Kit (Takara). The primers for rat PST were sense 5′-CCCATCACTGGTCTCCTCAT-3′ and antisense 5′-TTCTGTGAGGACTTGCGTTG-3′; for rat STX sense 5′-CGGGAATTCTGGAGGCAGAGGTACA-3 and antisense 5′-ATAATGTCTCCAGGCTTCAGGGTCC-3′; for rat GlcAT-P sense 5′-ACGCCCACCTACAGTAGACCGGTGC-3′ and antisense 5′-AAGGTCTCCCGCAACCAGCGCAGGG-3′; for rat GlcAT-S sense 5′-ATCATGTTGGACGTGGACCCCCG-CA-3′.

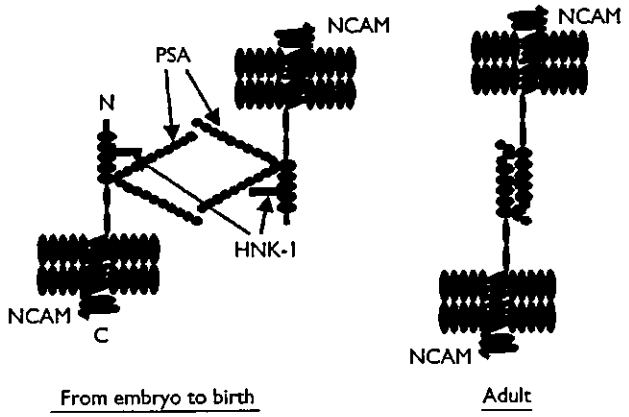

Fig. 1. A schematic representation of NCAM, PSA and HNK-1 carbohydrate epitopes. At the embryo stage (left), negative charge derived from PSA and HNK-1 carbohydrate epitopes interferes with the adhesion activity of NCAM, which contributes cell to cell adhesion in the adult (right).

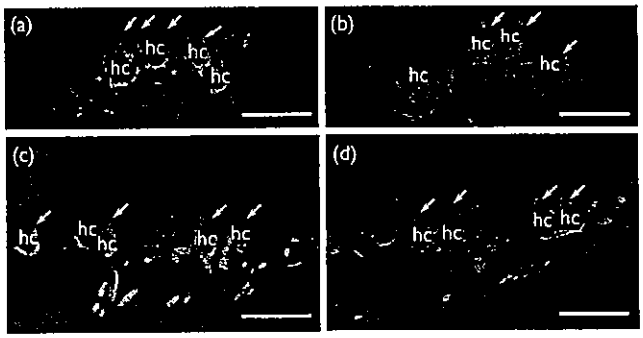

Fig. 2. Immunocytochemical localization of PSA (a,c) and HNK-1 carbohydrate epitopes (b,d) in the sensory epithelium of the rat crista ampullaris and macula utriculi. Immunoreactivities (arrows) around the hair cells (hc) correspond well with the known morphology of the nerve chalice (afferent nerve endings of type I hair cells). PSA and HNK-1 carbohydrate epitope-immunoreactive puncta, most probably afferent endings of type II hair cells, were also found beneath hair cells. Bar = 25 μm.

RESULTS

In the adult rat hippocampus, PSA and HNK-1 carbohydrate epitopes were immunocytochemically distributed in neurons in the dentate gyrus as described before (data not shown). These distribution patterns were in agreement with those of previous reports [10,11]. PSA and HNK-1 carbohydrate epitopes were found in all the vestibular endorgans (including crista ampullaris, macula utriculi, and macula sacculi). PSA and HNK-1 epitope immunoreactivities around the hair cells correspond well with the known morphology of the nerve chalice (afferent nerve endings of type I hair cells) (Fig. 2a–d). PSA and HNK-1 carbohydrate epitope-immunoreactive puncta, most probably afferent endings of type II hair cells, were also found beneath hair cells (Fig. 2a–d).

PSA and HNK-1 epitopes were co-localized in the hippocampus (data not shown) and the vestibular endorgans (Fig. 3a–c). PSA also co-localized with neurofilament 200, which is a marker of the afferent neurons (Fig. 3d–f). RT-PCR experiments revealed that two distinct types of polysialyltransferases, PST and STX, as well as two types of glucuronyltransferases, GlcAT-P and GlcAT-S, were transcribed in the hippocampus and the vestibular endorgans of adult rats (Fig. 4).

DISCUSSION

The present study clearly indicates that the vestibular endorgans of the adult rat are equipped with PSA and HNK-1 carbohydrate epitopes, unique glycans involved in structural plasticity. In addition, we have also shown that two polysialyltransferases, PST and STX, that independently form PSA, as well as two glucuronyltransferases, GlcAT-P and GlcAT-S, that independently synthesize HNK-1 epitopes, are transcribed in this particular organ. These results combined suggest that these developmentally regulated

Fig. 3. Double labeling for PSA (a: indicated by green) and HNK-1 (b: indicated by red) epitopes showing the two glycans are co-localized (c: indicated by yellow). Immunocytochemical double labeling of PSA (d: indicated by green) and neurofilament 200 (e: indicated by red) are co-localized in the nerve chalice (f: indicated by yellow). Bar=25 μm.

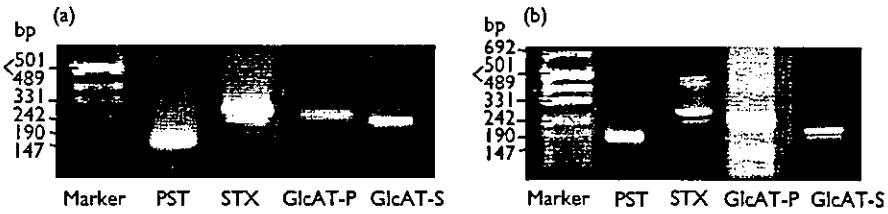

Fig. 4. RT-PCR analysis showing the existence of PST, STX, GlcAT-P and GlcAT-S mRNA in the hippocampus (a) and vestibular endorgans (b).

glycans, PSA and HNK-1 epitopes, are synthesized and still function in the adult vestibular endorgans in a manner similar to that suggested for the hippocampus, olfactory bulb, and cochlea.

PSA manifests in cell migration, neurite pathfinding, neurite outgrowth, and synaptic plasticity [1–3]. It has been speculated that polysialylated NCAM promotes weak adhesion of the cells. In addition, homophilic binding between highly polysialylated NCAMs is attenuated by the large negative charge of PSA, which is undetectable in most organs of the adult [12]. Decreased PSA in growing nerve fibers has been correlated with synapse formation [13].

In the adult, PSA was reported to be expressed in restricted areas, including the hippocampus, olfactory bulb [5], and cochlea [6], where neural rearrangement/plasticity is hypothesized to remain. According to Simonneau *et al.* [6], intense PSA immunoreactivity is found around the inner hair cells and at the base of outer hair cells in the developing cochlea which then gradually decreases after birth. PSA-NCAM expression was reported to be well correlated with synaptogenesis during cochlear development. Interestingly, immunoreactivity beneath inner hair cells remains even in adults (postnatal day 60). Simonneau *et al.* [6] hypothesized that PSA-NCAM, which is colocalized with GAP43 (a glycoprotein related to neuronal development and plasticity), has a potential role during dendritic regrowth and synaptic recovery.

Although it is not known whether vestibular endorgans have continuous neuronal plasticity, morphological evidence of synaptic rearrangement after exposure to microgravity has been demonstrated in vestibular endorgans [14,15], suggesting that potential plasticity of the vestibular system may occur even at the level of the hair cell region, as in the central nervous system [16,17]. According to Ross's observations, the number of synapses in type II hair cells is significantly increased after 9 days in space [14]. Our recent work also showed evidence that vestibular primary afferent neurons may have a potential role in neuronal plasticity [18]. In this study , CREB and syntaxin, which may reflect synaptic plasticity, are up-regulated after hypergravitational exposure. Interestingly, these two molecules were demonstrated in the primary afferent neurons.

The present study demonstrated that HNK-1 carbohydrate epitope, another glycan related to neuronal plasticity, is localized in the nerve calyx and co-localized with PSA. Strong expression of HNK-1 epitope has been reported in migrating neural crest cells and cerebellum [19,20]. Zhao *et al.* [21] demonstrated that during a short period after birth (PD3-10), HNK-1 epitope is strongly expressed in the granule cells of the external and internal granular layers of rat cerebellum, but the expression declines by postnatal day 15 and eventually disappears in adults. HNK-1 epitope is reported to be responsible for regulating the nervous system spatially and temporally during development [22,23]. These reports strongly suggested that HNK-1 as well as the NCAM-PSA system contributed to the plasticity and/or rearrangement of nerve cells. As shown in Fig. 1, PSA and HNK-1 epitopes interfere with the interaction between NCAMs by means of large negative charges of PSA and HNK-1 epitope from the embryonic stage to shortly after birth. In adulthood, the decreased amounts of PSA on NCAM facilitates the homophilic binding between NCAMs.

Our immunohistochemical findings showed co-localization of PSA and HNK-1 carbohydrate epitope in the primary afferent neurons in the vestibular endorgans of adult rats, suggesting that primary afferents may play an important role through these molecules. Although their most likely role would be a contribution to dendritic growth and synaptic recovery after damage in the hair cell region which is also hypothesized in the cochlea [6], the detailed role of these molecules requires further investigation.

CONCLUSION

The present findings indicated that NCAM-PSA and/or a HNK-1 system still remain even in adult peripheral endorgans as is seen in the hippocampus, olfactory bulb, and cochlea. PSA and HNK-1 carbohydrate epitope, co-localizing in the primary afferent neurons of the adult rat vestibular system, may have an important role in synaptic rearrangement and neuronal regrowth.

REFERENCES

1. Rutishauser U and Landmesser L. Polysialic acid in the vertebrate nervous system: a promoter of plasticity in cell-cell interactions. *Trends Neurosci* 1996; 19:422–427.
2. Fryer HJ and Hockfield S. The role of polysialic acid and other carbohydrate polymers in neural structural plasticity. *Curr Opin Neurobiol* 1996; 6:113–118.
3. Nakayama J, Angata K, Ong E, Katsuyama T and Fukuda M. Polysialic acid, a unique glycan that is developmentally regulated by two polysialyltransferases, PST and STX, in the central nervous system: from biosynthesis to function. *Pathol Int* 1998; 48:665–677.
4. Jungalwala FB. Expression and biological functions of sulfoglucuronyl glycolipids (SGGLs) in the nervous system – a review. *Neurochem Res* 1994; 19:945–957.
5. Ronn LC, Hartz BP and Bock E. The neural cell adhesion molecule (NCAM) in development and plasticity of the nervous system. *Exp Gerontol* 1998; 33:853–864.
6. Simonneau L, Gallego M and Pujol R. Comparative expression patterns of T-, N-, E-cadherins, β-catenin, and polysialic acid neural cell adhesion molecule in rat cochlea during development: implications for the nature of Kolliker's organ. *J Comp Neurol* 2003; 459:113–126.

7. Angata K and Fukuda M. Polysialyltransferases: major players in polysialic acid synthesis on the neural cell adhesion molecule. *Biochimie* 2003; 85:195–206.
8. Oka S, Terayama K, Kawashima C and Kawasaki T. A novel glucuronyltransferase in nervous system presumably associated with the biosynthesis of HNK-1 carbohydrate epitope on glycoproteins. *J Biol Chem* 1992; 267:22711–22714.
9. Imiya K, Ishizaki T, Seiki T, Saito F, Inazawa J, Oka S *et al.* cDNA cloning, genomic structure and chromosomal mapping of the mouse glucuronyltransferase-S involved in the biosynthesis of the HNK-1 carbohydrate epitope. *Gene* 2002; 296:29–36.
10. Seki T and Arai Y. The persistent expression of a highly polysialylated NCAM in the dentate gyrus of the adult rat. *Neurosci Res* 1991; 12: 503–513.
11. Yamamoto M, Marshall P, Hemmendinger LM, Boyer AB and Caviness VS Jr. Distribution of glucuronic acid-and-sulfate-containing glycoproteins in the central nervous system of the adult mouse. *Neurosci Res* 1988; 5:273–298.
12. Rutishauser U, Acheson A, Hall AK, Mann DM and Sunshine J. The neural cell adhesion molecule (NCAM) as a regulator of cell-cell interactions. *Science* 1988; 240:53–57.
13. Whitlon DS, Zhang X, Pecelunas K and Greiner MA. A temporospatial map of adhesive molecules in the organ of Corti of the mouse cochlea. *J Neurocytol* 1999; 28:955–968.
14. Ross MD. Changes in ribbon synapses and rough endoplasmic reticulum of rat utricular macular hair cells in weightlessness. *Acta Otolaryngol* 2000; 120:490–499.
15. Ross MD. A spaceflight study of synaptic plasticity in adult rat vestibular maculas. *Acta Otolaryngol Suppl* 1994; 516:1–14.
16. Igarashi M. Vestibular compensation. An overview. *Acta Otolaryngol Suppl* 1984; 406:78–82.
17. Curthoys IS and Halmagyi GM. Vestibular compensation. *Adv Otorhinolaryngol* 1999; 55:82–110.
18. Iijima N, Suzuki N, Oguchi T, Hashimoto S, Takumi Y, Sugahara K *et al.* The effect of hypergravity on the inner ear: CREB and syntaxin are up-regulated. *Neuroreport* 2004; 15:965–969.
19. Bronner-Fraser M. Analysis of the early stages of trunk neural crest migration in avian embryos using monoclonal antibody HNK-1. *Dev Biol* 1986; 115:44–55.
20. Eisenman LM and Hawkes R. Antigenic compartmentation in the mouse cerebellar cortex: zebrin and HNK-1 reveal a complex, overlapping molecular topography. *J Comp Neurol* 1993; 335:586–605.
21. Zhao Z, Chou DK, Nair SM, Tobet S and Jungalwala FB. Expression of sulfoglucuronyl (HNK-1) carbohydrate and its binding protein (SBP-1) in developing rat cerebellum. *Brain Res Dev Brain Res* 2000; 120:165–180.
22. Schwarting GA, Jungalwala FB, Chou DK, Boyer AM and Yamamoto M. Sulfated glucuronic acid-containing glycoconjugates are temporally and spatially regulated antigens in the developing mammalian nervous system. *Dev Biol* 1987; 120:65–76.
23. Yoshihara Y, Oka S, Watanabe Y and Mori K. Developmentally and spatially regulated expression of HNK-1 carbohydrate antigen on a novel phosphatidylinositol-anchored glycoprotein in rat brain. *J Cell Biol* 1991; 115:731–744.

Acknowledgements: We thank A.C. Apple-Mathews for help in preparing the manuscript. This work was supported by the Ground Research for Space Utilization program of NASDA and the Japan Space Forum (S.U.), and Grants-in-Aid for Scientific Research from the Ministry of Education, Culture, Sports, Science and Technology of Japan (Y.T., J.N.).

Reprint Series

Science

13 August 2004

Vol. 305 No. 5686
Pages 901–1060 $10

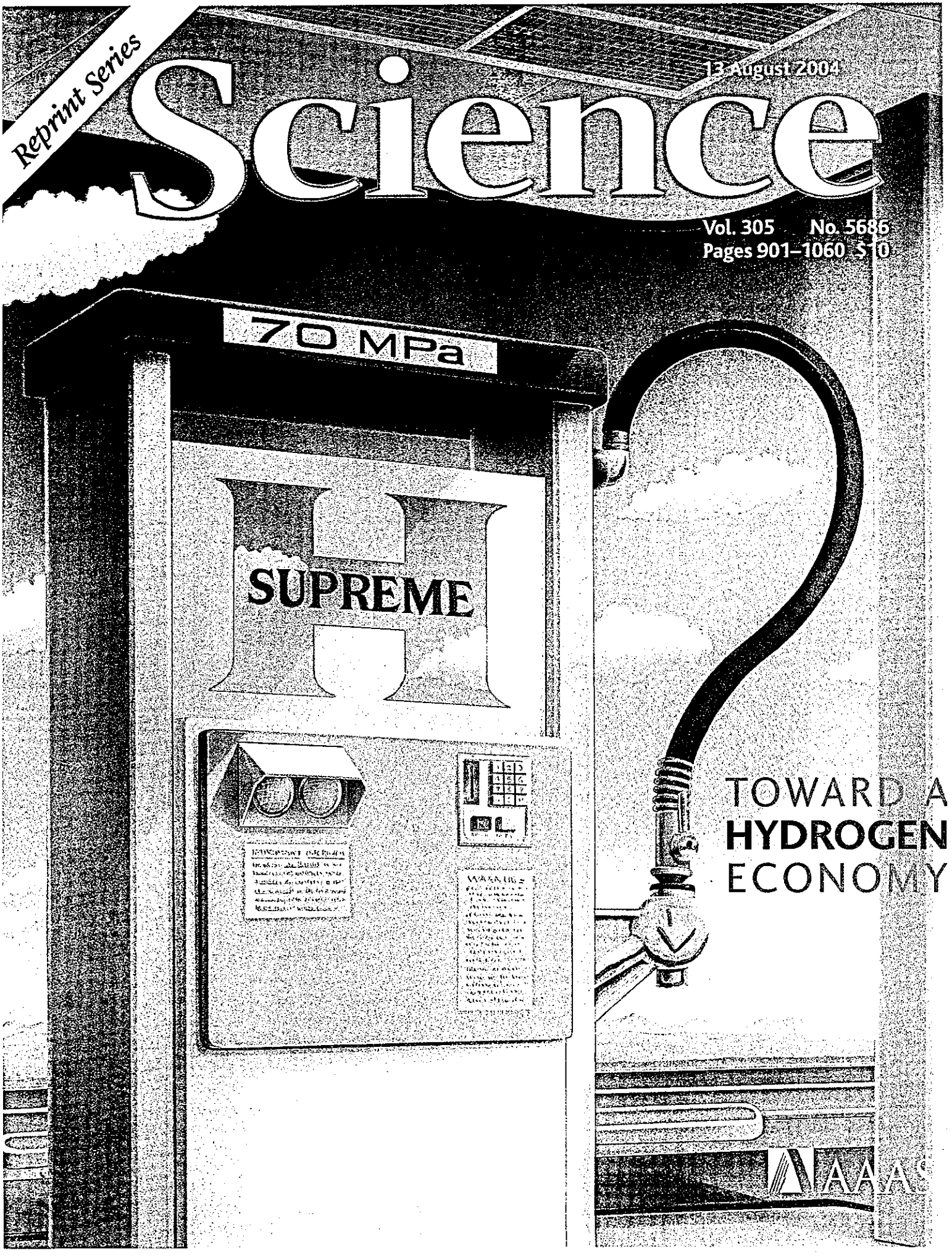

TOWARD A HYDROGEN ECONOMY

AAAS

Natural Antibiotic Function of a Human Gastric Mucin Against *Helicobacter pylori* Infection

Masatomo Kawakubo,[1,2] Yuki Ito,[1] Yukie Okimura,[2] Motohiro Kobayashi,[1,4] Kyoko Sakura,[2] Susumu Kasama,[1] Michiko N. Fukuda,[4] Minoru Fukuda,[4] Tsutomu Katsuyama,[2] Jun Nakayama[1,3]*

Helicobacter pylori infects the stomachs of nearly a half the human population, yet most infected individuals remain asymptomatic, which suggests that there is a host defense against this bacterium. Because *H. pylori* is rarely found in deeper portions of the gastric mucosa, where O-glycans are expressed that have terminal α1,4-linked *N*-acetylglucosamine, we tested whether these O-glycans might affect *H. pylori* growth. Here, we report that these O-glycans have antimicrobial activity against *H. pylori*, inhibiting its biosynthesis of cholesteryl-α-D-glucopyranoside, a major cell wall component. Thus, the unique O-glycans in gastric mucin appeared to function as a natural antibiotic, protecting the host from *H. pylori* infection.

Helicobacter pylori colonizes the gastric mucosa of about half the world's population and is considered a leading cause of gastric malignancies (*1–3*). However, most infected individuals remain asymptomatic or are affected merely by chronic active gastritis (*2*). Only a fraction of infected patients develop peptic ulcer, gastric cancer, and malignant lymphoma. This suggests the presence of host defense mechanisms against *H. pylori* pathogenesis.

Gastric mucins are classified into two types based on their histochemical properties (*4*). The first is a surface mucous cell–type mucin, secreted from the surface mucous cells. The second is found in deeper portions of the mucosa and is secreted by gland mucous cells, including mucous neck cells, cardiac gland cells, and pyloric gland cells.

In *H. pylori* infection, the bacteria are associated solely with surface mucous cell–type mucin (*5*), and two carbohydrate structures, Lewis b and sialyl dimeric Lewis X in surface mucous cells, serve as specific ligands for *H. pylori* adhesins, BabA and SabA, respectively (*6, 7*). *H. pylori* rarely colonizes the deeper portions of gastric mucosa, where the gland mucous cells produce mucins having terminal α1,4-linked *N*-acetylglucosamine (α1,4-GlcNAc) residues attached to core 2–branched *O*-glycans [GlcNAcα1→4Galβ1→4GlcNAcβ1→6(GlcNAcα1→ 4Galβ1→3)GalNAcα→Ser/Thr] (*8*). Development of pyloric gland atrophy enhances the risk of peptic ulcer or gastric cancer two- to three-fold compared with chronic gastritis without pyloric gland atrophy (*3*). These findings raise the possibility that α1,4-GlcNAc–capped *O*-glycans have protective properties against *H. pylori* infection.

To test this hypothesis, we generated mucin-type glycoproteins containing terminal α1,4-GlcNAc and determined its effect on *H. pylori* in vitro. Because CD43 serves as a preferential core protein of these *O*-glycans (*8*), we generated recombinant soluble CD43 having α1,4-GlcNAc–capped *O*-glycans in transfected Chinese hamster ovary cells (*9*). Soluble CD43 without α1,4-GlcNAc was used as a control.

H. pylori (ATCC43504), incubated with the medium containing varying amounts of recombinant soluble CD43, showed little growth during the first 2.5 days, irrespective of the presence or absence of α1,4-

[1]Department of Pathology and [2]Department of Laboratory Medicine, Shinshu University School of Medicine, and [3]Institute of Organ Transplants, Reconstructive Medicine and Tissue Engineering, Shinshu University Graduate School of Medicine, Asahi 3-1-1, Matsumoto 390-8621, Japan. [4]Glycobiology Program, Cancer Research Center, The Burnham Institute, 10901 North Torrey Pines Road, La Jolla, CA 92037, USA.

*To whom correspondence should be addressed. E-mail: jun@hsp.md.shinshu-u.ac.jp

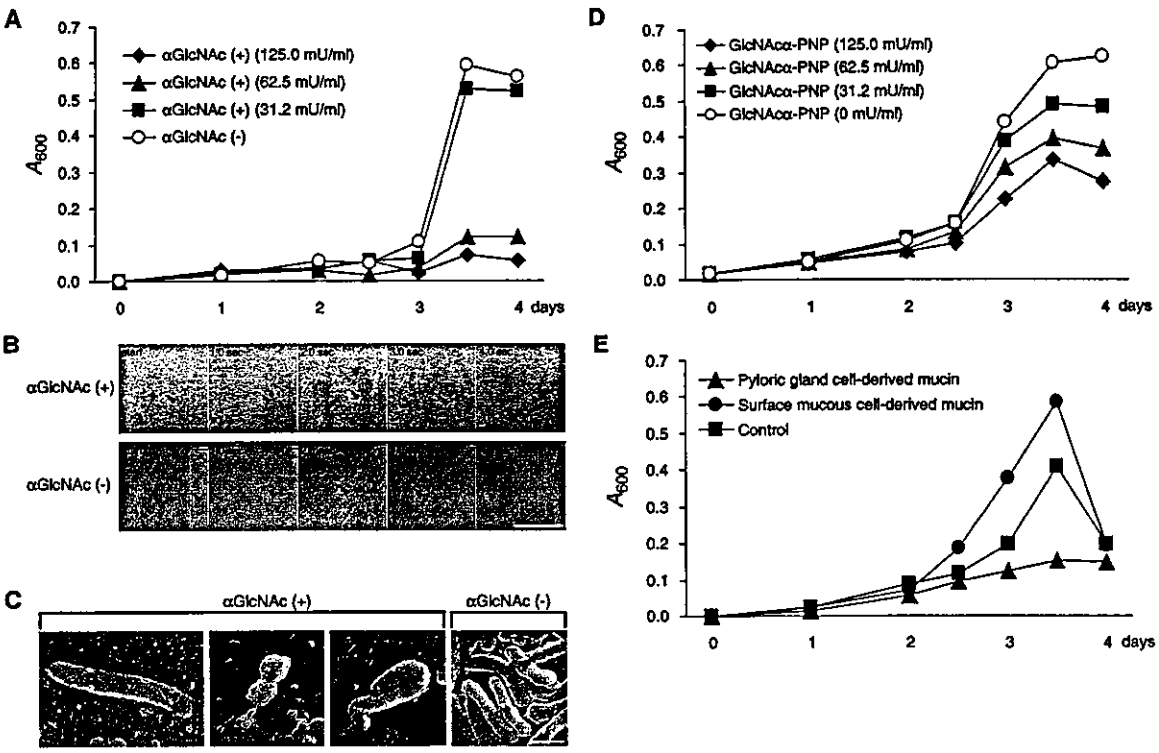

Fig. 1. α1,4-GlcNAc–capped *O*-glycans inhibit the growth and motility of *H. pylori*. (**A**) Growth curves of *H. pylori* cultured in the presence of soluble CD43 with terminal α1,4-GlcNAc [αGlcNAc (+)] or soluble CD43 without terminal α1,4-GlcNAc [αGlcNAc (–)]; the protein concentration of αGlcNAc (–) was the same as that of 125.0 mU/ml of αGlcNAc (+). One miliunit of αGlcNAc (+) corresponds to 1 μg (2.9 nmol) of GlcNAcα-PNP. A_{600}, absorbance at 600 nm. (**B**) Motility of *H. pylori* cultured with 31.2 mU/ml of αGlcNAc (+) or the same protein concentration of αGlcNAc (–) for 3 days by time-lapse recording with 1-s intervals. Representative *H. pylori* is indicated by arrowheads. The mean velocity of seven *H. pylori* cultured in the presence of αGlcNAc (+) and αGlcNAc (–) is 3.1 ± 3.5 μm/s (mean ± SD) and 21.2 ± 2.6 μm/s ($P < 0.001$). Scale bar, 50 μm. (**C**) Scanning electron micrographs of *H. pylori* incubated with 31.2 mU/ml of αGlcNAc (+) or the same protein concentration of αGlcNAc (–) for 3 days. Note abnormal morphologies such as elongation, segmental narrowing, and folding in the culture with αGlcNAc (+). All photographs were taken at the same magnification. Scale bar, 1 μm. (**D**) Growth curves of *H. pylori* cultured in the medium supplemented with various amounts of GlcNAcα-PNP. Growth of the bacteria is suppressed by GlcNAcα-PNP in a dose-dependent manner. (**E**) Growth curves of *H. pylori* cultured in the medium supplemented with pyloric gland cell-derived mucin containing 125 mU/ml of α1,4-GlcNAc or the same protein concentration of surface mucous cell-derived mucin isolated from the human gastric mucosa. The death phase started from 3.5 days, and saline instead of each mucin was supplemented as a control experiment. In (A), (D), and (E), each value represents the average of duplicate measurements.

GlcNAc–capped *O*-glycans, characteristic of the lag phase of *H. pylori* growth (Fig. 1A). After 3 days, microbes cultured in the presence of control soluble CD43 grew rapidly, corresponding to the log phase of bacterial growth. In contrast, soluble CD43 containing more than 62.5 mU/ml of terminal α1,4-GlcNAc impaired log-phase growth. Although growth inhibition was not obvious at a lower concentration (31.2 mU/ml), time-lapse images of the microbes revealed significant reduction of motility under this condition (Fig. 1B). Morphologic examination at the lower concentration revealed abnormalities of the microbe, such as elongation, segmental narrowing, and folding (Fig. 1C). These morphologic changes are distinct from conversion to coccoid form, because reduction of growth, associated with conversion from the bacillary to the coccoid form (*10*), was not apparent under these conditions. These inhibitory effects of soluble CD43 containing terminal α1,4-GlcNAc were also detected against various *H. pylori* strains, including another authentic strain, ATCC43526, and three clinical isolates with a minimum inhibitory concentration between 15.6 mU/ml and 125.0 mU/ml. By contrast, neither inhibitory growth nor abnormal morphology of *H. pylori* was observed at any concentrations of soluble CD43 lacking α1,4-GlcNAc (Fig. 1, A to C). These results indicate that α1,4-GlcNAc–capped *O*-glycans specifically suppress the growth of *H. pylori* in a manner similar to other antimicrobial agents. Similar inhibitory effects on *H. pylori* were also found in another mucin-like glycoprotein, CD34 (*11*) having terminal α1,4-GlcNAc (*12*). In addition, *p*-nitrophenyl-α-*N*-acetylglucosamine (GlcNAcα-PNP) suppressed the growth of *H. pylori* in a dose-dependent manner (Fig. 1D), although the effects were not as strong with soluble CD43 having terminal α1,4-GlcNAc (Fig. 1A). These results provide evidence that the terminal α1,4-GlcNAc residues, rather than scaffold proteins, are critical for growth inhibitory activity against *H. pylori*, and that the presentation of multiple terminal α1,4-GlcNAc residues as a cluster on mucin-type glycoprotein may be important for achieving the optimal activity.

To determine whether natural gastric mucins containing terminal α1,4-GlcNAc can also inhibit growth of *H. pylori*, subsets of human gastric mucins were prepared from the surface mucous cells and pyloric gland cells (*9*). The growth of *H. pylori* was significantly suppressed with mucin derived from pyloric gland cells at 125.0 mU/ml during the log phase (Fig. 1E). A similar inhibitory effect was also observed when the glandular mucin prepared from human gastric juice was tested (*13*). By contrast, mucin derived from surface mucous cells, MUC5AC, stimulated growth. These results support the hypothesis that natural gastric mucins containing terminal α1,4-GlcNAc, secreted from gland mucous cells, have antimicrobial activity against *H. pylori*.

The morphologic abnormalities of *H. pylori* induced by α1,4-GlcNAc–capped *O*-glycans are similar to those induced by antibiotics such as β-lactamase inhibitors, which disrupt biosynthesis of peptidoglycan in the cell wall (*14, 15*). Therefore, these *O*-glycans may inhibit cell wall biosynthesis in *H. pylori*. The cell wall of

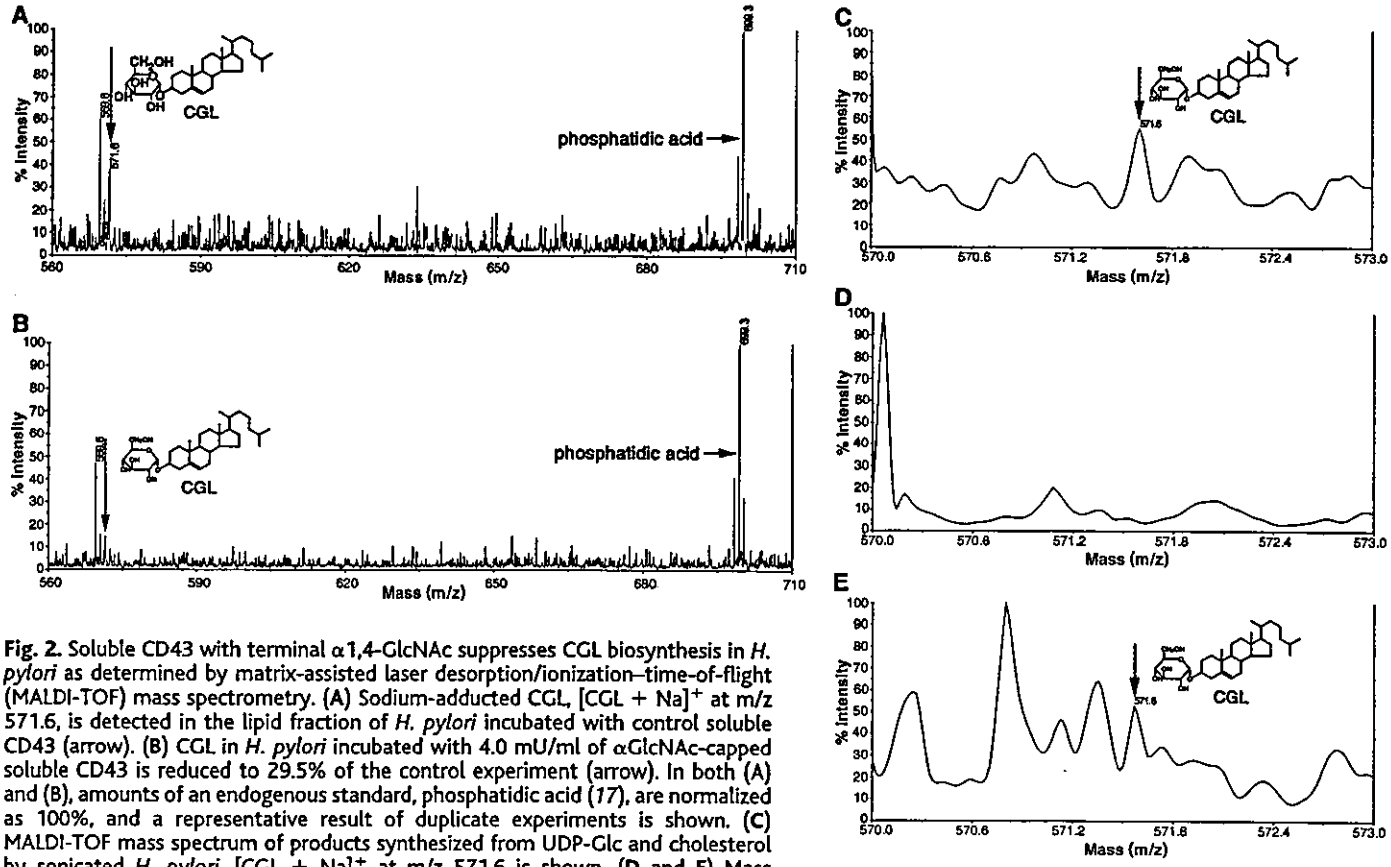

Fig. 2. Soluble CD43 with terminal α1,4-GlcNAc suppresses CGL biosynthesis in *H. pylori* as determined by matrix-assisted laser desorption/ionization–time-of-flight (MALDI-TOF) mass spectrometry. (**A**) Sodium-adducted CGL, $[CGL + Na]^+$ at m/z 571.6, is detected in the lipid fraction of *H. pylori* incubated with control soluble CD43 (arrow). (**B**) CGL in *H. pylori* incubated with 4.0 mU/ml of αGlcNAc-capped soluble CD43 is reduced to 29.5% of the control experiment (arrow). In both (**A**) and (**B**), amounts of an endogenous standard, phosphatidic acid (*17*), are normalized as 100%, and a representative result of duplicate experiments is shown. (**C**) MALDI-TOF mass spectrum of products synthesized from UDP-Glc and cholesterol by sonicated *H. pylori*. $[CGL + Na]^+$ at m/z 571.6 is shown. (**D** and **E**) Mass spectrum of products synthesized from UDP-Glc and cholesterol by sonicated *H. pylori* in the presence of 50.0 mU/ml of α1,4-GlcNAc–capped soluble CD43 (D) or control soluble CD43 (E). Note that CGL is not synthesized in the presence of α1,4-GlcNAc–capped soluble CD43 in (D).

Fig. 3. Absence of α-CGs including CAG, CGL, and CPG in *H. pylori* cultured without exogenous cholesterol. Total glycolipids extracted from *H. pylori* incubated with Brucella broth lacking cholesterol (lane 1) or containing 0.005% cholesterol (lane 2) were analyzed by thin-layer chromatography.

Helicobacter species characteristically contains α-cholesteryl glucosides (α-CGs), of which the major components are cholesteryl-α-D-glucopyranoside (CGL), cholesteryl-6-*O*-tetradecanoyl-α-D-glucopyranoside (CAG), and cholesteryl-6-*O*-phosphatidyl-α-D-glucopyranoside (CPG) (*16*). Mass spectrometric analysis of the cell wall components from *H. pylori* cultured with α1,4-GlcNAc–capped *O*-glycans displayed reduced lipid-extractable cell wall constituents (Fig. 2B). In particular, the levels of CGL, relative to phosphatidic acid (*17*), were significantly reduced as compared with controls (Fig. 2, A and B). These results suggest that α1,4-GlcNAc–capped *O*-glycans directly inhibit biosynthesis of CGL in vivo by *H. pylori*.

CGL is likely formed by a UDP-Glc:sterol α-glucosyltransferase, which transfers glucose (Glc) from UDP-Glc to the C3 position of cholesterol with α-linkage. Incubation of cholesterol and UDP-Glc with *H. pylori* lysates revealed substantial amounts of CGL by mass spectrometry (Fig. 2C), demonstrating the activity of UDP-Glc:sterol α-glucosyltransferase in *H. pylori*. When soluble CD43 containing terminal α1,4-GlcNAc was added to this assay, production of CGL was suppressed (Fig. 2D), whereas no effect was seen with control soluble CD43 (Fig. 2E). Considering structural similarity between α-linked GlcNAc found in the gland mucous cell–type mucin and the α-linked Glc found in CGL, these findings suggest that the terminal α1,4-GlcNAc residues could directly inhibit the α-glucosyltransferase activity through an end-product inhibition mechanism (*18*), resulting in decreased CGL biosynthesis.

Genes involved in the biosynthesis of cholesterol are not found in the genome database of *H. pylori* (*19*). Thus, *H. pylori* may not be able to synthesize CGL in the absence of exogenous cholesterol. When *H. pylori* was cultured for 5 days without cholesterol, bacterial growth was significantly reduced (table S1). In such cultures, *H. pylori* was elongated and no motile microbes were found. When *H. pylori* was further cultured without cholesterol for up to 21 days, the microbes died off completely. By contrast, when *H. pylori* was cultured with cholesterol, bacteria grew well, and no signs of abnormality were detected (table S1). *H. pylori* cultured with cholesterol (*9*) revealed a typical triplet of α-CGs including CGL (Fig. 3, lane 2), while α-CGs were not detected in *H. pylori* cultured without cholesterol (Fig. 3, lane 1). Moreover, no antibacterial effect of soluble CD43 containing terminal α1,4-GlcNAc was observed on bacterial strains lacking CGL such as *Escherichia coli*, *Pseudomonas aeruginosa*, *Klebsiella pneumoniae*, *Staphylococcus aureus*, α-*Streptococcus*, and *Streptococcus pneumoniae* (*9*). These results collectively indicate that synthesis of CGL by using exogenously supplied cholesterol is required for the survival of *H. pylori* and that antimicrobial activity of α1,4-GlcNAc–capped *O*-glycans may be restricted to bacterial strains expressing CGL.

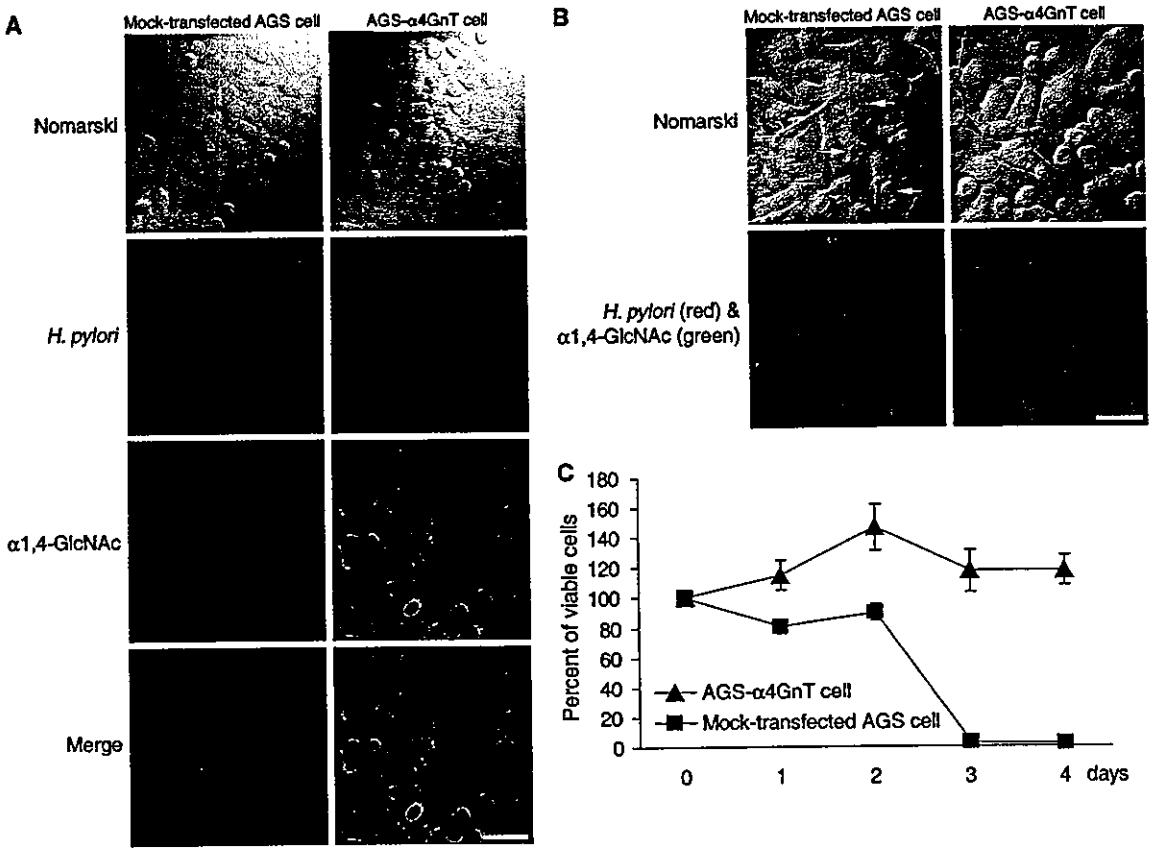

Fig. 4. α1,4-GlcNAc–capped *O*-glycans protect the host cells. AGS cells were incubated with *H. pylori* for 8 hours (A) or 24 hours (B), and doubly stained with anti-*H. pylori* antibody (red) and HIK1083 antibody specific for terminal α1,4-GlcNAc (*27*) (green). (A) Note that comparable number of *H. pylori* adhered to both mock-transfected AGS cells and AGS-α4GnT cells. (B) After 24 hours, marked damage such as cell flatness or shrinkage are noted (arrows) in mock-transfected AGS cells; no cellular damage and few attached bacteria are found in AGS-α4GnT cells. (Top) Nomarski photographs of the same field. Scale bar, 50 μm. (C) Viabilities of AGS cells cocultured with *H. pylori* for 4 days determined by MTS assay. Note that viability of mock-transfected AGS cells was significantly reduced after the third day, whereas AGS-α4GnT cells were fully viable for up to 4 days. The assay was done with triplicate measurements, and error bars indicate SD.

To test whether mucous cells expressing α1,4-GlcNAc–capped *O*-glycans protect themselves against *H. pylori* infection, gastric adenocarcinoma AGS-α4GnT cells stably transfected with α4GnT cDNA were cocultured with *H. pylori* (*9*). With a short-term incubation (8 hours), the microbes attached equally well to AGS-α4GnT cells and mock-transfected AGS cells. No significant damage was observed in either group of cells (Fig. 4A). Upon prolonged incubation (24 hours), mock-transfected AGS cells exhibited remarkable deterioration, such as flatness or shrinkage, with increased number of associated *H. pylori* (Fig. 4B), and the number of viable AGS cells was dramatically reduced after the third day (Fig. 4C). This cellular damage may be attributed to the perturbed signal transduction in AGS cells, where a tyrosin phosphatase, SHP-2, is constitutively activated by *H. pylori* CagA protein (*20*). By contrast, growth of *H. pylori* in cultures with AGS-α4GnT cells was markedly suppressed, and cellular damage found in mock-transfected AGS cells was barely detected in these cells (Fig. 4B). Thus, the viability of AGS-α4GnT cells was fully maintained for up to 4 days (Fig. 4C). These results indicate that α1,4-GlcNAc–capped *O*-glycans have no effect on the adhesion of *H. pylori* to AGS-α4GnT cells, but protect the host cells from *H. pylori* infection.

Glycan chains play diverse roles as ligands for cell surface receptors (*11*, *21*–*23*) and as modulators of receptors and adhesive proteins (*24*–*26*). The present study reveals a new aspect of mammalian glycan function as a natural antibiotic. Because α1,4-GlcNAc–capped *O*-glycans are produced by human gastric gland mucous cells, the present study provides a basis for development of novel and potentially safe therapeutic agents to prevent and treat *H. pylori* infection in humans without adverse reactions.

References and Notes

1. R. M. Peek Jr., M. J. Blaser, *Nature Rev. Cancer* **2**, 28 (2002).
2. D. R. Cave, *Semin. Gastrointest. Dis.* **12**, 196 (2001).
3. P. Sipponen, H. Hyvarinen, *Scand. J. Gastroenterol. Suppl.* **196**, 3 (1993).
4. H. Ota *et al.*, *Histochem. J.* **23**, 22 (1991).
5. E. Hidaka *et al.*, *Gut* **49**, 474 (2001).
6. D. Iiver *et al.*, *Science* **279**, 373 (1998).
7. J. Mahdavi *et al.*, *Science* **297**, 573 (2002).
8. J. Nakayama *et al.*, *Proc. Natl. Acad. Sci. U.S.A.* **96**, 8991 (1999).
9. Materials and methods are available as supplemental material on *Science* Online.
10. H. Enroth *et al.*, *Helicobacter* **4**, 7 (1999).
11. J.-C. Yeh *et al.*, *Cell* **105**, 957 (2001).
12. M. Kawakubo, J. Nakayama, unpublished observations.
13. Y. Ito, M. Kawakubo, J. Nakayama, unpublished observations.
14. T. Horii *et al.*, *Helicobacter* **7**, 39 (2002).
15. J. Finlay, L. Miller, J. A. Poupard, *J. Antimicrob. Chemother.* **52**, 18 (2003).
16. Y. Hirai *et al.*, *J. Bacteriol.* **177**, 5327 (1995).
17. Y. Inamoto *et al.*, *J. Clin. Gastroenterol.* **17**, S136 (1993).
18. J. Nakayama *et al.*, *J. Biol. Chem.* **271**, 3684 (1996).
19. J. F. Tomb *et al.*, *Nature* **388**, 539 (1997).
20. H. Higashi *et al.*, *Science* **295**, 683 (2002).
21. J. B. Lowe, *Cell* **104**, 809 (2001).
22. T. O. Akama *et al.*, *Science* **295**, 124 (2002).
23. N. L. Perillo, K. E. Pace, J. J. Seilhamer, L. G. Baum, *Nature* **378**, 736 (1995).
24. D. J. Moloney *et al.*, *Nature* **406**, 369 (2000).
25. M. Demetriou, M. Granovsky, S. Quaggin, J. W. Dennis, *Nature* **409**, 733 (2001).
26. J. Nakayama, M. N. Fukuda, B. Fredette, B. Ranscht, M. Fukuda, *Proc. Natl. Acad. Sci. U.S.A.* **92**, 7031 (1995).
27. K. Ishihara *et al.*, *Biochem. J.* **318**, 409 (1996).

28. This work was supported by a Grant-in-Aid for Scientific Research on Priority Area 14082201 from the Ministry of Education, Culture, Sports, Science and Technology of Japan (J.N.) and by grants CA 71932 (M.N.F.) and CA 33000 (M.F.) from the National Cancer Institute. The authors thank H. Ota, Y. Kawakami, T. Taketomi, and O. Harada for discussions; E. Ruoslahti, R. C. Liddington, and E. Lamar for critical reading of the manuscript; and E. Hidaka, Y. Takahashi, S. Kubota, and A. Ishida for technical assistance. This report is dedicated to the memory of Hideki Matsumoto.

Supporting Online Material

www.sciencemag.org/cgi/content/full/305/5686/1003/DC1

Materials and Methods

Table S1

References and Notes

16 April 2004; accepted 21 June 2004

Journal of Neuro-Oncology 68: 217–223, 2004.

Laboratory Investigation

Inducible expression of $p57^{KIP2}$ inhibits glioma cell motility and invasion

Sakai K[1], Peraud A[4], Mainprize T[4], Nakayama J[2], Tsugu A[3], Hongo K[1], Kobayashi S[1] and James T. Rutka[4]

[1]*Department of Neurosurgery, Shinshu University School of Medicine;* [2]*Department of Organ Regeneration, Institutes of Organ Transplants, Reconstructive Medicine and Tissue Engineering, Shinshu University Graduate School of Medicine;* [3]*Department of Neurosurgery, Tokai University School of Medicine;* [4]*The Arthur and Sonia Labatt Brain Tumour Research Centre, The Hospital for Sick Children, and the Division of Neurosurgery, University of Toronto, Canada*

Key words: invasion assay, motility assay, $p57^{KIP2}$

Summary

To examine the role of $p57^{KIP2}$ in human malignant glioma cells, we studied its expression in a panel of human malignant glioma specimens by western blot and immunohistochemical analysis. To determine the effects of $p57^{KIP2}$ expression on the phenotype of glioma cells, we analyzed two inducible stably transfected $p57^{KIP2}$ expressing glioma cell lines. Expression of $p57^{KIP2}$ was induced in U373 and U87 malignant glioma cells with doxycycline using the tetracycline repressor system. A phagokinetic track assay on gold particles was used to investigate differences in cell migration between $p57^{KIP2}$ expressing and non-expressing control cells. The effects of the extracellular matrix (ECM) on U373 motility was determined in $p57^{+}$ and $p57^{-}$cells on surfaces coated with 5 $\mu g/cm^2$ of fibronectin, laminin, type I and type IV collagens. The invasion of $p57^{+}$ and $p57^{-}$ glioma cells across BD Biocoat Matrigel invasion chambers was then determined. $p57^{KIP2}$ was weakly expressed in 4/6 glioblastoma (GBM) specimens by western blot. By immunohistochemistry, $p57^{KIP2}$ immunoreactivity was positive in 8/40 GBMs, and was primarily nuclear in location. The motility of U373 glioma cells was significantly reduced after $p57^{KIP2}$ induction. The presence of ECM proteins did not further alter the motility of $p57^{+}$ and $p57^{-}$ glioma cells. The results of the invasion chamber assay showed that $p57^{+}$ cells exhibited a 35% reduction in their invasive capacity as compared to $p57^{-}$ cells. These data suggest that $p57^{KIP2}$ is expressed in at least some malignant gliomas. Inducible expression of 57^{KIP2} in cell lines deficient in this cyclin-dependent kinase inhibitor reduces their motility and invasiveness.

Introduction

The malignant potential of astrocytic brain tumors derives from their highly proliferative and invasive nature [1,2]. It is well known that malignant astrocytomas acquire numerous genetic alterations that ultimately affect cell cycle control [3–5]. Important positive regulators of the cell cycle are the cyclin-dependent kinases (CDKs) which phosphorylate key intermediary protein species such as the retinoblastoma protein (RB) which promote release from cell cycle arrest. In contrast, cyclin-dependent kinase inhibitors (CDKIs) such as $p57^{KIP2}$ can potentially arrest the cell in various phases of the cell cycle, and if deleted, may act as tumor suppressor genes [6,7].

It has been hypothesized that migration and proliferation are mutually exclusive cellular programs in invasive gliomas [8,9]. Previous results from our laboratory indicated that $p57^{KIP2}$ overexpression in malignant glioma cell lines significantly decreases cellular proliferation and promotes cell scenescence [5]. The purpose of the present study was to focus on the migratory and

invasive potential of malignant glioma cells under the influence of $p57^{KIP2}$ expression, and to determine whether the above described dichotomous cellular behavior holds for glioma cells expressing this CDKI.

Materials and methods

Cells, cell culture, and tumor specimens

U373 MG (U373) and U87 human malignant glioma cells were a generous gift of Bengt Westermark (Uppsala, Sweden) [10]. These two cell lines do not express endogenous $p57^{KIP2}$ [5]. The p57-positive SJCRH30 rhabdomyosarcoma cell line was a generous gift of Peter Dirks, The Hospital for Sick Children. The cells were maintained in alpha minimal essential medium (MEM) containing 10% fetal bovine serum and penicillin/streptomycin/fungizone (Gibco BRL, Grand Island, NY) in a humidified atmosphere of 5% CO_2 in air at 37 °C. Glioblastoma multiforme (GBM) surgical specimens were obtained from the Toronto Western Hospital brain tumor bank. Permission to use these specimens was approved by the Research Ethics Board at the Toronto Western Hospital, The University of Toronto.

Plasmids and transfection

Plasmids and the method of transfection were described previously [5]. The tetracycline-regulated gene expression system was used to induce expression of $p57^{KIP2}$ [11–13]. pUHD10-3 is the tetracycline-regulated expression vector under the control of a human cytomegalovirus (hCMV) minimal promoter (generously provided by Dr. H. Bujard, Heidelberg, Germany) [13–16].

U373 and U87 cells were first transfected with the pUHD172-1 neo plasmid (25 μg) (generously provided by Dr. H. Bujard, Heidelberg, Germany) containing the reverse transactivator (rtTA) coding sequence downstream of the hCMV promoter/enhancer and *neo* marker, using the calcium phosphate method. Neomycin-resistant clones were selected in 0.9 mg/ml of geneticin (G418, Gibco BRL, Gaithersburg, MD) and stable expression of the fusion protein was determined by Western blot analysis of total cell lysates using a polyclonal antisera to VP 16 (generously provided by Dr. C.J. Ingles, Toronto, Canada). Clones that demonstrated high-level expression of VP 16 were used for transfection with pUHD10-3. A full-length human $p57^{KIP2}$ cDNA (kind gift of S.J. Elledge, Houston, TX) was inserted into the multiple cloning site of pUHD10-3, and this plasmid (25 μg) was co-transfeccted with *pgk*-puro (1 μg) for transfection of stable cell lines. Puromycin (Sigma, St. Louis, MO) was used for selection at 1 μg/ml and G418 concentration was maintained at 500 μg/ml.

To induce expression of $p57^{KIP2}$, the $p57^{KIP2}$-transfected U373 and U87 cells were maintained in 4 μg/ml of doxycycline (Sigma, St. Louis, MO) added from a 4 mg/ml stock in 70% ethanol.

Phagokinetic track assay

Uniform gold particles were prepared on 35-mm Falcon plastic culture plates (Falcon Plastics, Division of BioQuest, Oxnard, Calif.) coated with 1% BSA according to the method of Albrecht-Buehler [13–19]. In this assay, during cell attachment, spreading and locomotion, cells remove gold particles from the substrate. One thousand $p57^{KIP2}$- transfected U373 or U87 cells were seeded per dish in routine medium with or without doxycycline. The cells were incubated for 24 h at 37 °C in a humidified incubator with 5% CO_2, and then fixed with 4% formaldehyde in PBS. Phagokinetic tracks were examined in a Digital HD Microscope (VH-7000, Keyence, Pleasanton, CA), and photographs were taken. Tracks were outlined and measured in pixels using the NIH Image 1.59 program. The mean area of 50 tracks per dish was determined.

For the investigation of the effects of extracellular matrix (ECM) constituents on U373 migration, fibronectin (Becton Dickinson, Bedford, MA), laminin (Becton Dickinson, Bedford, MA), collagen type I (Becton Dickinson, Bedford, MA) and collagen type IV (Becton Dickinson, Bedford, MA) coated dishes were used at defined concentrations (5 $\mu g/cm^2$). Gold particles were then plated on each dish and the phagokinetic track assay was applied as described above. The motility of $p57^{KIP2}$-induced and uninduced U373 glioma cells was then determined on these ECM components.

Invasion assay

The invasion assay was performed by using 24-well BD Biocoat Matrigel invasion chambers with 8-μm polycarbonated filters (Becton Dickinson, Bedford, MA), as described by Albini et al. [20]. Five thousand $p57^{KIP2}$- transfected U373 cells were seeded on Matrigel invasion chamber plates, and cultured in routine medium in the absence or presence of doxycycline. Cells were incubated for 20 h at 37 °C in a humidified incubator with 5% CO_2. Nonmigratory cells on the upper surface of the filter were removed by wiping with a cotton swab. Invasive cells that penetrated through pores and migrated to the underside of the membrane were stained with Giemsa solution after fixation with 4% formaldehyde in PBS. The cell number was counted under microscopic vision, and the average cell number was determined.

Western blot analysis

GBM specimens were suspended in NP-40 Lysis Buffer (1% NP-40, 20 mM Tris pH 7.4, 150 mM NaCl, 5 mM EDTA) and homogenized. The samples were centrifuged, the supernatant was removed and the protein concentration obtained using BioRad Protein Assay (Bio-Rad Laboratories, Hercules, CA, USA). Forty microgram of total protein lysates were resolved on 10% SDS-PAGE gels and electrophoretically transferred to polyvinylidene fluoride (PVDF) membranes (Millipore, Bedford, MA). Membranes were blocked with 5% (w/v) skim milk powder in 1× Tris-buffered saline with 0.05% Tween 20 for 30 min prior to the antibody addition. Blocked membranes were incubated for 1 h at room temperature with mouse anti-human $p57^{KIP2}$ antibody (BD Bioscience, San Jose, CA) at a dilution of 1:300 and mouse anti-actin antibody (Sigma, St. Louis, MO) at a dilution of 1:2000. Membranes were incubated with horseradish peroxidase (HRP) conjugated secondary antibody (BioRad, Hercules, CA) at room temperature for 45 min at a dilution of 1:5000. Bound antibody was detected using enhanced chemiluminescence reagent (ECL, Perkin-Elmer, Boston, MA). The p57-positive cell line, SJCRH30, was used as a positive control in the western blot analysis.

Immunohistochemistry

Forty formalin-fixed, paraffin-embedded GBMs were used for immunohistochemical analysis. Five micrometer tissue sections were mounted on positively charged microscope slides. Tissue sections were then baked over night @ 60 °C, dewaxed in xylene and hydrated to distilled water through decreasing concentrations of alcohol.

All tissue sections were treated with heat induced epitope retrieval (HIER) and blocked for endogenous peroxidase and biotin. The counterstain of preference was haematoxylin. Immunohistochemical procedures were performed for mouse anti-human $p57^{KIP2}$ antibody at 1:200 (Santa Cruz, Santa Cruz, CA).

Statistical analysis

P values were calculated using the Student's *t* test, and error bars represent standard deviation. Each assay was performed in triplicate, with each sample tested in triplicate.

Results

Inducible expression of $p57^{KIP2}$ reduces cell motility

$p57^{KIP2}$ was expressed under the control of the tetracycline operator (tetO) in U373 and U87 cell lines that constitutively express high levels of the tetracycline repressor (tetR)-VP16 fusion protein [5]. In the presence of doxycycline, p57 is identified by western blot analysis, whereas in its absence, it is not [5] (data not shown). Tracks produced by motile cells were depicted with a digital microscope (Figure 1). The track size of U373 and U87 cells that were transfected and induced to express $p57^{KIP2}$ were markedly smaller and less irregular than those of control cells in which the $p57^{KIP2}$ gene was not expressed in the absence of doxycycline in the culture medium. The mean track size per dish (pooled from 50 measurements) was significantly smaller in cells overexpressing $p57^{KIP2}$ compared to control cells ($P < 0.001$) (Figure 2A and B). In addition, the area of the tracks outlined by moving cells was significantly reduced by 63.8% in U373 cells and by 68% in U87 cells expressing $p57^{KIP2}$.

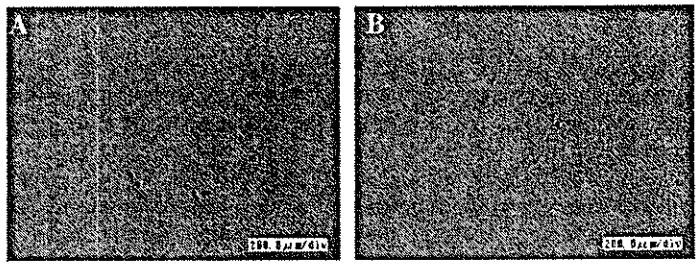

Figure 1. Phagokinetic tracks of U373 glioma cells on gold-coated dishes. (A) U373 glioma cell tracks from cells grown in the absence of doxycycline (p57$^-$). (B) U373 glioma cell tracks from cells grown in the presence of doxycycline (p57$^+$). Bar = 200 μm.

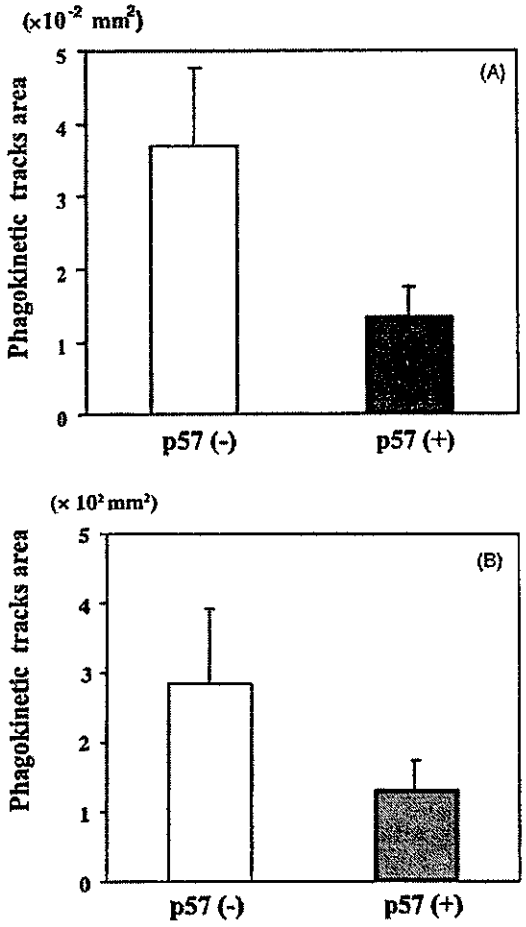

Figure 2. Computer-assisted calculations of track areas from the phagokinetic assay. Induction of p57 in U373 (A) and U87 (B) glioma cells reduces track size area when compared to p57$^-$ cells ($P < 0.001$). Error bars indicate standard deviation.

Effects of p57^{KIP2} on U373 motility is independent of the extracellular matrix

To determine whether the effect of p57^{KIP2} is dependent on the extracellular matrix on which U373 cells were growing, we further investigated their phagokinetic behaviour on different ECM substrates such as fibronectin, laminin, collagen type I and IV. p57^{KIP2} expression did not influence U373 astrocytoma cell motility on different matrix components when compared to controls. Irrespective of ECM substrate, induced expression of p57^{KIP2} led to a 50–55% smaller track area on phagokinetic assays than did controls (data not shown).

Overexpression of p57 reduces the invasiveness of U373 cells

The Matrigel invasion chamber was used to measure the fraction of tumor cells expressing p57^{KIP2} capable of invading through a matrix of reconstituted basement membrane compared to controls. Invading U373 cells were scored, and only 65% of those that expressed p57^{KIP2} were found to invade Matrigel-coated filters in comparison to 100% of control cells (Figure 3). This difference was statistically significant ($P < 0.005$).

Expression of p57^{KIP2} in Glioma specimens

Western blot analysis of p57^{KIP2} demonstrated slight expression in four of six fresh frozen GBM samples (Figure 4). Lysate from the rhabdomyosarcoma cell line SJCRH30 was used as a positive control. Eight of the 40 GBM samples demon-

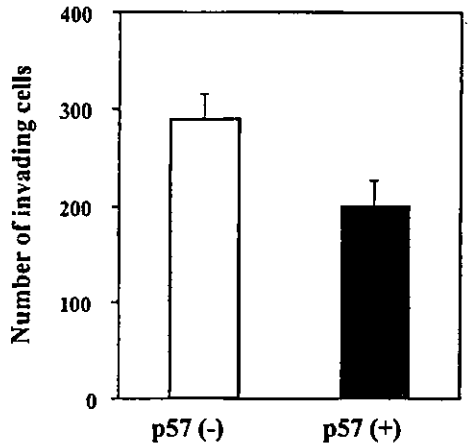

Figure 3. Invasion assay on Matrigel-coated filters. U373 glioma cells expressing p57 were significantly inhibited from crossing Matrigel coated filters than were $p57^-$ cells ($P < 0.005$).

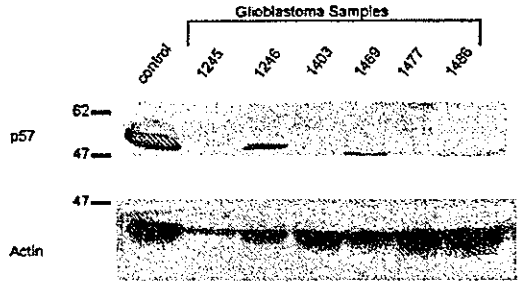

Figure 4. Western blot analysis of $p57^{KIP2}$ in Glioblastoma Multiforme. Four of the GBM specimens demonstrate weak expression of $p57^{KIP2}$. Actin blot below serves as a control for protein loading. Lane 1 control = p57-positive SJCRH30 rhabdomyosarcoma cell line; Lane 2–7 – Different GBM specimens.

strated $p57^{KIP2}$ expression and was found to be primarily nuclear in these tumors (Figure 5).

Discussion

In the present study, $p57^{KIP2}$ was induced in U373 and U87 glioma cells to investigate its impact on cell motility. Using a phagokinetic assay to measure tumor cell track size on gold-coated surfaces, we show that $p57^{KIP2}$ expression inhibited glioma cell motility. Motility was not affected by growing $p57^+$ and $p57^-$ U373 cells on substrata of single ECM macromolecules. However, the invasion of $p57^+$ U373 glioma cells was markedly inhibited when placed on matrigel-coated filters. Taken together, these data show that the inducible expression of $p57^{KIP2}$, a CDKI, by p57-negative glioma cells reduces their motility and invasion.

Previous studies have shown that $p57^{KIP2}$ is expressed in fetal brain tissue, but not in astrocytic tumors of varying grades or permanent astrocytoma cell lines. We have shown that the induction of $p57^{KIP2}$ in U373, U343, and U87 cells rapidly arrests cell growth in the G1 phase of the cell cycle [5]. The effect of $p57^{KIP2}$ on reducing the number of viable cells was previously shown to be greater among U373 than among U343 glioma cells. Interestingly, a population of U373 astrocytoma cells responded to the induction of $p57^{KIP2}$ by undergoing apoptosis. In addition, $p57^{KIP2}$-induced astrocytoma cells were shown to undergo distinct morphological changes becoming large and flat and having abundant cytoplasm. In essence, these astrocytoma cells exhibited a cell scenescent phenotype.

Interestingly, there have been several studies that demonstrate a dichotomous cellular behavior with regard to migration and proliferation [21–23] with enhanced proliferation when motility was inhibited and *vice versa*. In contrast, our results here suggest that $p57^{KIP2}$ overexpression simultaneously downregulates proliferation and migration. A recent report of Yoshizato et al. studied the influence of the specific thromboxane synthase inhibitor furegrelate, and also showed an inhibition of motility and decreased cell growth in five different human glioma cell lines [9]. They concluded that the regulation of motility through eicosanoids might involve a different signaling pathway than those activated by cell–matrix interactions.

In order to determine the influence of several ECM components on tumor cell migration we grew $p57^{KIP2}$ transfected U373 cells on fibronectin, laminin, collagen type I and IV, but did not find any significant difference between $p57^{KIP2}$ expressing or control cells. These results suggest that the ECM components studied here had no impact on U373 cell motility in the phagokinetic

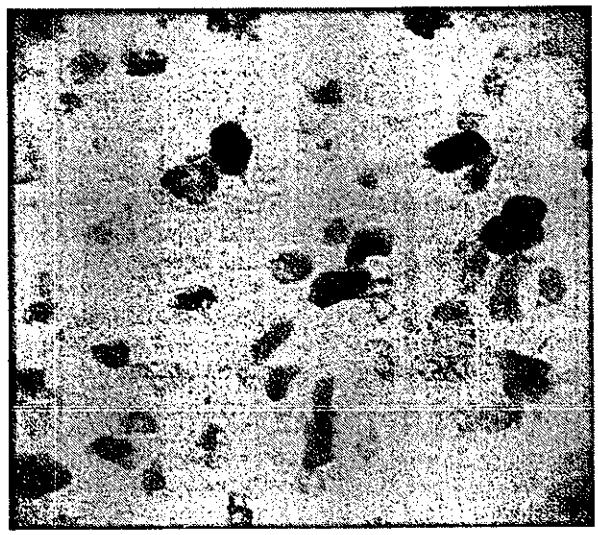

Figure 5. Immunohistochemical staining of $p57^{KIP2}$ in GBM. There is significant $p57^{KIP2}$ immunoreactivity in the nuclei of many of the tumor cells. Magnification ×375.

assay utilized. Giese et al. described a higher migration rate of seven human glioma cell lines on merosin and tenascin than on collagen, fibronectin or vitronectin [8]. When an aggregate mixture of ECM macromolecules was tested in the Matrigel invasion assay, $p57^+$ U373 glioma cells were significantly inhibited from crossing the prepared membranes.

To place the role of $p57^{KIP2}$ expression in malignant gliomas into some context, we showed that 4/6 GBM tumor specimens express this CDKI, albeit weakly. Furthermore, we examined 40 malignant gliomas by immunohistochemistry for $p57^{KIP2}$. Eight GBMs showed immunoreactivity for $p57^{KIP2}$. The predominant staining pattern of $p57^{KIP2}$ was nuclear in these tumors which may reflect its importance in cell cycle control. Different studies have shown $p57^{KIP2}$ immunoreactivity to be a positive prognostic factor for pancreatic, hepatocellular and ovarian carcinomas [6, 24–26].

In summary, the present study shows that the inducible expression of $p57^{KIP2}$ in the U373 and U87 astrocytoma cell lines is able to significantly reduce cell motility and invasion. These findings may have potential implications for the further study of the role of cell cycle inhibitors in targeting glioma cell growth, motility and invasion. These data suggest that providing a strong proliferative block to U373 and U87 glioma cells will not lead to a migratory or invasive cell phenotype among $p57^+$ expressing cells. Our future studies are aimed at continuing to explore the role of controlling glioma cell growth by re-introducing $p57^{KIP2}$ into p57-negative glioma cells in animal model systems, and at further determining the relationship between $p57^{KIP2}$ expression and outcome for patients harbouring malignant gliomas.

Acknowledgements

Aurelia Peraud was funded by the Deutsche Forschungsgemeinschaft (Pe 758/2-1). James Rutka is a Scientist of the Canadian Institutes of Health Research (CIHR). This work was supported in part by grants from the CIHR, the Laurie Berman and Wiley Funds for Brain Tumor Research, and Brainchild.

References

1. Holland EC: Glioblastoma multiforme: the terminator. Proc Natl Acad Sci USA 97: 6242–6244, 2000

2. Louis DN, Holland EC, Cairncross JG: Glioma classification: a molecular reappraisal. Am J Pathol 159: 779–786, 2001
3. Dirks PB, Hubbard SL, Murakami M, Rutka JT: Cyclin and cyclin-dependent kinase expression in human astrocytoma cell lines. J Neuropathol Exp Neurol 56: 291–300, 1997
4. Dirks PB, Rutka JT: Current concepts in neuro-oncology: the cell cycle – a review. Neurosurgery 40: 1000–1013, 1997 (discussion 1013–1005)
5. Tsugu A, Sakai K, Dirks PB, Jung S, Weksberg R, Fei YL, Mondal S, Ivanchuk S, Ackerley C, Hamel PA et al.: Expression of p57(KIP2) potently blocks the growth of human astrocytomas and induces cell senescence. Am J Pathol 157: 919–932, 2000
6. Mainprize TG, Taylor MD, Rutka JT, Dirks PB: Cip/Kip cell-cycle inhibitors: a neuro-oncological perspective. J Neurooncol 51: 205–218, 2001
7. Matsuoka S, Edwards MC, Bai C, Parker S, Zhang P, Baldini A, Harper JW, Elledge SJ: p57KIP2, a structurally distinct member of the p21CIP1 Cdk inhibitor family, is a candidate tumor suppressor gene. Genes Dev 9: 650–662, 1995
8. Giese A, Loo MA, Rief MD, Tran N, Berens ME: Substrates for astrocytoma invasion. Neurosurgery 37: 294–301, 1995 (discussion 301–292)
9. Yoshizato K, Zapf S, Westphal M, Berens ME, Giese A: Thromboxane synthase inhibitors induce apoptosis in migration-arrested glioma cells. Neurosurgery 50: 343–354, 2002
10. Westermark B, Ponten J, Hugosson R: Determinants for the establishment of permanent tissue culture lines from human gliomas. Acta Pathol Microbiol Scand [A] 81: 791–805, 1973
11. Baron U, Gossen M, Bujard H: Tetracycline-controlled transcription in eukaryotes: novel transactivators with graded transactivation potential. Nucleic Acids Res 25, 2723–2729, 1997
12. Gossen M, Bujard H: Studying gene function in eukaryotes by conditional gene inactivation. Annu Rev Genet 36: 153–173, 2002
13. Gossen M, Bujard H: Tight control of gene expression in mammalian cells by tetracycline-responsive promoters. Proc Natl Acad Sci USA 89: 5547–5551, 1992
14. Gossen M, Bujard H: Efficacy of tetracycline-controlled gene expression is influenced by cell type: commentary. Biotechniques 19: 213–216, 1995. (Discussion 216–217)
15. Gossen M, Freundlieb S, Bender G, Muller G, Hillen W, Bujard H: Transcriptional activation by tetracyclines in mammalian cells. Science 268, 1766–1769, 1995
16. Resnitzky D, Gossen M, Bujard H, Reed SI: Acceleration of the G1/S phase transition by expression of cyclins D1 and E with an inducible system. Mol Cell Biol 14: 1669–1679, 1994
17. Albrecht-Buehler G: The phagokinetic tracks of 3T3 cells. Cell 11: 395–404, 1977
18. Albrecht-Buehler G: Phagokinetic tracks of 3T3 cells: parallels between the orientation of track segments and of cellular structures which contain actin or tubulin. Cell 12: 333–339, 1977
19. Albrecht-Buehler G: The tracks of moving cells. Sci Am 238, 68–76, 1978
20. Albini A, Iwamoto Y, Kleinman HK, Martin GR, Aaronson SA, Kozlowski JM, McEwan RN: A rapid in vitro assay for quantitating the invasive potential of tumor cells. Cancer Res 47: 3239–3245, 1987
21. Giese A, Loo MA, Tran N, Haskett D, Coons SW, Berens ME: Dichotomy of astrocytoma migration and proliferation. Int J Cancer 67: 275–282, 1996
22. Mariani L, Beaudry C, McDonough WS, Hoelzinger DB, Demuth T, Ross KR, Berens T, Coons SW, Watts G, Trent JM et al.: Glioma cell motility is associated with reduced transcription of proapoptotic and proliferation genes: a cDNA microarray analysis. J Neurooncol 53: 161–176, 2001
23. Mariani L, Beaudry C, McDonough WS, Hoelzinger DB, Kaczmarek E, Ponce F, Coons SW, Giese A, Seiler RW, Berens ME: Death-associated protein 3 (Dap-3) is overexpressed in invasive glioblastoma cells in vivo and in glioma cell lines with induced motility phenotype in vitro. Clin Cancer Res 7: 2480–2489, 2001
24. Ito Y, Takeda T, Sakon M, Tsujimoto M, Monden M, Matsuura N: Expression of p57/Kip2 protein in hepatocellular carcinoma. Oncology 61: 221–225, 2001
25. Nakai S, Masaki T, Shiratori Y, Ohgi T, Morishita A, Kurokohchi K, Watanabe S, Kuriyama S: Expression of p57(KIP2) in hepatocellular carcinoma: relationship between tumor differentiation and patient survival. Int J Oncol 20: 769–775, 2002
26. Rosenberg E, Demopoulos RI, Zeleniuch-Jacquotte A, Yee H, Sorich J, Speyer JL, Newcomb EW: Expression of cell cycle regulators p57(KIP2), cyclin D1, cyclin E in epithelial ovarian tumors and survival. Hum Pathol 32: 808–813, 2001

Address for offprints: James T. Rutka, The Division of Neurosurgery, Suite 1502, The Hospital for Sick Children, 555 University Avenue, Toronto, Ontario, Canada M5G 1X8; Tel.: +1-416-813-4975; Fax: +1-416-813-4975; E-mail: james.rutka@sickkids.ca

Induction of peripheral lymph node addressin in human gastric mucosa infected by *Helicobacter pylori*

Motohiro Kobayashi*†, Junya Mitoma*, Naoshi Nakamura‡, Tsutomu Katsuyama§, Jun Nakayama†, and Minoru Fukuda*¶

*Glycobiology Program, Cancer Research Center, The Burnham Institute, La Jolla, CA 92037; and Departments of †Pathology, ‡Internal Medicine, and §Laboratory Medicine, Shinshu University School of Medicine, Matsumoto 390-8621, Japan

Edited by Stuart A. Kornfeld, Washington University School of Medicine, St. Louis, MO, and approved November 9, 2004 (received for review October 9, 2004)

Helicobacter pylori **infects over half the world's population and is a leading cause of peptic ulcer and gastric cancer. *H. pylori* infection results in chronic inflammation of the gastric mucosa, and progression of chronic inflammation leads to glandular atrophy and intestinal metaplasia. However, how this chronic inflammation is induced or maintained is not well known. Here, we show that chronic inflammation caused by *H. pylori* infection is highly correlated with *de novo* synthesis of peripheral lymph node addressin (PNAd) presented on high-endothelial venule (HEV)-like vessels. The number of HEV-like vessels dramatically increases as chronic inflammation progresses. We found that the PNAd is bound by L-selectin-IgM chimeric protein, and decorated by NCC-ST-439 antibody, which is suggested to recognize both nonsulfated and 6-sulfated sialyl Lewis X on core 2 branched O-glycans, and MECA-79 antibody, which reacts with 6-sulfo *N*-acetyllactosamine on extended core 1 O-glycans. These results indicate that PNAd on HEV-like vessels present in the gastric mucosa subsequent to *H. pylori* infection is similar to those on HEVs present in the secondary lymphoid organs, which are essential for lymphocyte circulation. Moreover, eradication of *H. pylori* is associated with the disappearance of HEV-like vessels in the gastric mucosa. By contrast, very few PNAd were found in the gastric mucosa of patients with chemical gastritis caused by nonsteroidal antiinflammatory drugs. These results strongly suggest that PNAd in HEV-like vessels plays a critical role in lymphocyte recruitment during chronic inflammation induced by *H. pylori* infection.**

inflammation | peptic ulcers | gastric carcinoma

Helicobacter pylori is a Gram-negative microaerophilic bacterium that infects >50% of the world's population (1). The infection of *H. pylori* is usually confined to the surface mucous cell-derived mucin (2). If untreated, this infection leads to chronic active gastritis and develops pyloric gland atrophy and intestinal metaplasia expressing intestine-specific genes, including MUC2, sucrase/isomaltase, and carbonic anhydrase 1 (3–7). This second advanced stage of gastritis is closely associated with the pathogenesis of peptic ulcers.

The host responds to *H. pylori* infection primarily by mounting a strong neutrophilic response. Such a response contributes to gastric epithelial damage and is followed by chronic inflammatory infiltrates composed of lymphocytes and plasma cells, forming mucosa-associated lymphoid tissue (8). Although it has not been formally proven, it is suggested that this mucosal inflammation in response to *H. pylori* infection might lead to gastric carcinoma and malignant lymphoma (4, 5, 9–11). It is thus important to understand how lymphocytes are recruited to the gastric mucosa during the progression of chronic inflammation. However, such mechanisms are not fully understood.

In chronic inflammatory states of other systems, L-selectin and its ligands are implicated in lymphocyte recruitment in those diseases for which peripheral lymph node addressin (PNAd) is induced on high-endothelial venule (HEV)-like vessels (12, 13). Such HEV-like vessels have been observed in rheumatoid arthritis, lymphocytic thyroiditis, and inflammatory bowel diseases (14–17). In these studies, the induction of PNAd is detected by MECA-79 antibody (18), which decorates PNAd on HEV-like vessels. Indeed, BCA-1, a homing chemokine in the lymphoid tissue, and MECA-79-positive vessels were detected in mucosa-associated lymphoid tissue associated with *H. pylori* infection (19, 20).

MECA-79$^+$ HEVs in the secondary lymphoid organs play a major role in lymphocyte circulation (12). The MECA-79 epitope has been shown to be 6-sulfo *N*-acetyllactosamine attached to extended core 1 O-glycans, Galβ1→4(SO_3→6) GlcNAcβ1→3Galβ1→3GalNAcα1→Ser/Thr (21). Moreover, MECA-79 antibody can also bind to its sialylated and fucosylated form that constitutes PNAd (21). Structural studies also showed that 6-sulfo sialyl Lewis X on core 2 branched O-glycans, sialic acid-α2→3Galβ1→4[Fucα1→3(SO_3→6)]GlcNAcβ1→6 (Galβ1→3) GalNAcα1→Ser/Thr is present as a major L-selectin ligand on HEVs (21, 22).

In the present study, we found that inflammatory response to *H. pylori* infection is associated with the formation of HEV-like vessels in the gastric mucosa. HEV-like vessels express PNAd, characterized by binding to MECA-79, HECA-452 (23), and NCC-ST-439 (24) antibodies, and L-selectin-IgM chimeric protein. The expression of HEV-like vessels, assessed by MECA-79 and HECA-452 antibody staining, was highly correlated with the degree of lymphocyte infiltration. Moreover, we show that HEV-like vessels disappear once *H. pylori* is eradicated. These results indicate that inflammatory response to *H. pylori* infection is, at least in part, facilitated by induction of PNAd, thereby recruiting lymphocytes to the gastric mucosa.

Materials and Methods

Histological Specimens. We retrieved 143 formalin-fixed, paraffin-embedded blocks of histological specimens with various degrees of chronic gastritis from the archives of the Department of Laboratory Medicine, Shinshu University Hospital. Tissue sections 3 μm thick were stained with hematoxylin and eosin. Based on the updated Sydney system (25), gastritis was evaluated by using a visual analogue scale to evaluate five factors, including (*i*) *H. pylori* density, (*ii*) polymorphonuclear neutrophil activity, (*iii*) chronic infiltration of lymphocytes, (*iv*) glandular atrophy, and (*v*) intestinal metaplasia. Each factor was categorized into four grades: normal, mild, moderate, and marked. This grading

This paper was submitted directly (Track II) to the PNAS office.

Abbreviations: HEV, high-endothelial venule; PNAd, peripheral lymph node addressin; NSAID, nonsteroidal antiinflammatory drug; LSST, L-selectin ligand sulfotransferase; FucT-VII, fucosyltransferase VII; Core1-β3GlcNAcT, core 1 extension β1,3-*N*-acetylglucosaminyltransferase; Core2GlcNAcT-I, core 2 β1,6-*N*-acetylglucosaminyltransferase I; PSGL-1, P-selectin glycoprotein ligand 1.

¶To whom correspondence should be addressed at: The Burnham Institute, 10901 North Torrey Pines Road, La Jolla, CA 92037. E-mail: minoru@burnham.org.